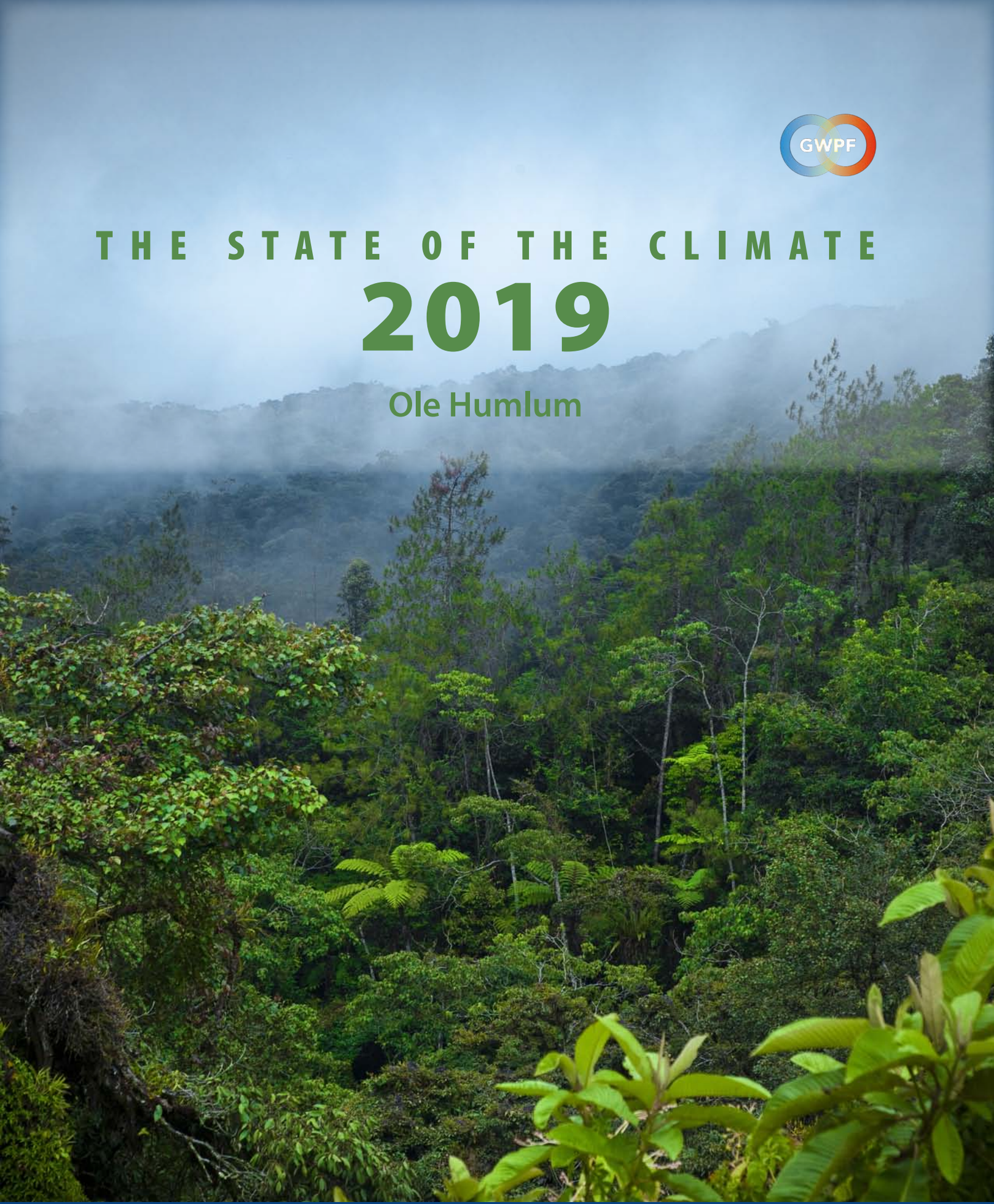

THE STATE OF THE CLIMATE 2019

Ole Humlum

The Global Warming Policy Foundation
Report 42

The State of the Climate 2019

Ole Humlum

Report 42, The Global Warming Policy Foundation

ISBN 978-1-8380747-0-8

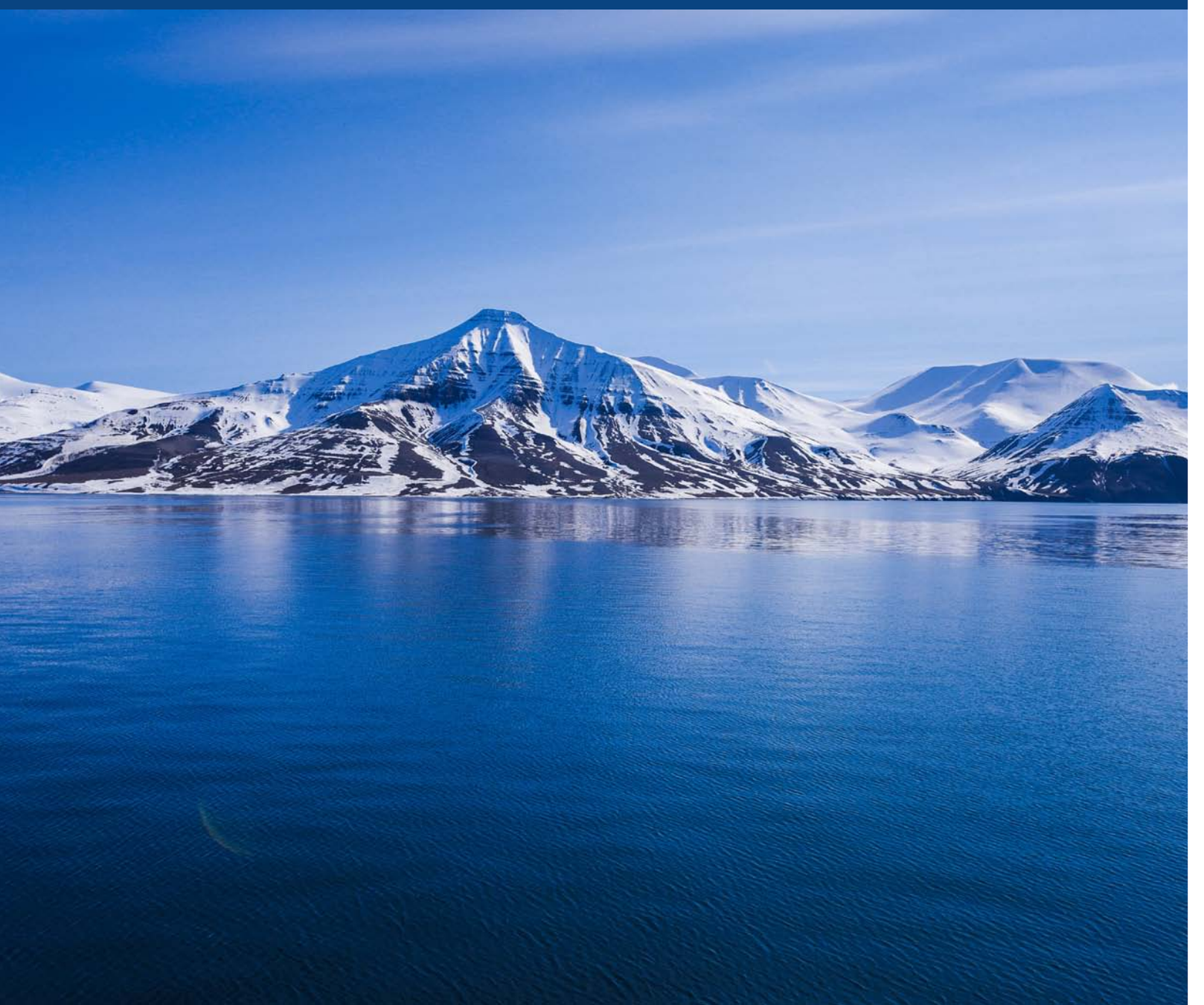

Contents

About the author

Ole Humlum is former Professor of Physical Geography at the University Centre in Svalbard, Norway, and Emeritus Professor of Physical Geography, University of Oslo, Norway.

Executive summary; the ten key facts

1. According to the instrumental temperature record (since about 1850), 2019 was a very warm year, but cooler than 2016.

2. In 2019, the average global air temperature was affected by a moderate El Niño episode, interrupting a gradual global air temperature decrease following the strong 2015–16 El Niño.

3. Since 1979, lower troposphere temperatures have increased over both land and oceans, but more so over land areas. The possible explanations include insolation, cloud cover and land use.

4. The temperature variations recorded in the lowermost troposphere are generally reflected at higher altitudes too. In the stratosphere, however, a temperature 'pause' commenced in around 1995, 5–7 years before a similar temperature 'pause' began in the lower troposphere near the planet's surface. The stratospheric temperature 'pause' has now persisted for about 25 years.

5. The 2015–16 oceanographic El Niño was among the strongest since the beginning of the record in 1950. Considering the entire record, however, recent variations between El Niño and La Niña are not unusual.

6. Since 2004, when detailed recording of ocean temperatures began, the global oceans above 1900 m depth have, on average, warmed somewhat. The strongest warming (between the surface and 200 m depth) mainly affects the oceans near the Equator, where the incoming solar radiation is at its maximum. In contrast, for the North Atlantic, net cooling at the surface has been pronounced since 2004.

7. Data from tide gauges all over the world suggest an average global sea-level rise of 1–1.5 mm/year, while the satellite record suggests a rise of about 3.2 mm/year, or more. The noticeable difference in rate (a ratio of at least 1:2) between the two data sets still has no broadly accepted explanation.

8. Since 1979, Arctic and Antarctic sea-ice extents have had opposite trends, decreasing and increasing, respectively. Superimposed on these overall trends, however, variations of shorter duration are also important in understanding year-to-year variations. In the Arctic, a 5.3-year periodic variation is important, while for the Antarctic a variation of about 4.5-years' duration is seen. Both these variations reached their minima simultaneously in 2016, which explains the simultaneous minimum in global sea-ice extent. This particularly affected Antarctic sea-ice extent in 2016.

9. Northern Hemisphere snow cover extent undergoes important local and regional variations from year to year. Since 1972, however, snow extent has been largely stable.

10. Tropical storms and hurricanes have displayed large annual variations in accumulated cyclone energy (ACE) since 1970, but there has been no overall trend towards either lower or higher activity. The same applies for the number of continental hurricane landfalls in the USA, in a record going back to 1851.

1. General overview 2019

The focus in this report is on observations, and not on output from numerical models. All references and data sources are listed at the end.

Air temperatures

Air temperatures measured near the planet's surface are at the core of many climate deliberations, but the significance of short-term warming or cooling in surface air temperatures should not be overstated. Whenever the Earth experiences warm El Niño or cold La Niña episodes, major heat exchanges take place between the Pacific Ocean and the atmosphere above, eventually showing up as a signal in the global air temperature. However, such a change does not reflect a change in the total heat content of the ocean–atmosphere system, instead chiefly reflecting redistribution of energy between the ocean and atmosphere. Evaluating the dynamics of ocean temperatures is therefore at least as important as evaluating changes in surface air temperatures.

Considering the entire surface air temperature record since 1850 or 1880, 2019 was a very warm year, but in all global temperature records it was cooler than 2016. However, the decrease in temperatures characterising 2017 and 2018 was interrupted by a renewed, moderate El Niño episode, underlining the importance of ocean–atmosphere exchanges.

Many Arctic regions experienced record high air temperatures in 2016, but since then, including in 2019, conditions have generally been cooler. The Arctic temperature peak in 2016 may have been affected by ocean heat released from the Pacific Ocean during the strong 2015–16 El Niño and subsequently transported northwards. This underscores how Arctic air temperatures may not only be affected by variations in local conditions, but also by changes far away.

Many diagrams in this report focus on the period since 1979 – the satellite era – in which we have a wide range of observations with nearly global coverage, including temperature. These data provide a detailed view of temperature changes over time at different altitudes in the atmosphere. These observations reveal that while the relatively well-known lower troposphere temperature pause began around 2002, a similar stratospheric temperature plateau had already begun back in 1995, several years before the start of a similar plateau in surface temperatures.

Since 1979, lower troposphere temperatures have increased over both land and oceans, but most clearly over land. The most uncomplicated explanation for this is that much of the warming is caused by solar insolation, but there may well be several supplementary reasons, such as, changes in cloud cover and land use.

Ocean temperatures

The Argo program has now achieved 15 years of global coverage, growing from a relatively sparse array of 1000 floats in 2004 to more than 4000 in early 2020. Deployment of new floats continues at the rate of up to 800 per year. The floats have delivered a unique ocean temperature dataset for depths down to 1900 m (although the oceans are much deeper than that). Despite this limitation and the fact that the data series is still relatively short, interesting features are now emerging from the observations.

Since 2004, the upper 1900 m of the oceans have experienced net warming, considering the global average. The maximum warming (0.08–0.23°C) affects the uppermost 200 m of the oceans, and mainly in regions near the Equator, where the greatest amount of solar radiation is received. At greater depths, a small (about 0.02°C) net warming occurred between 2004 and 2019.

The warming mainly affected the Equatorial

oceans between 30°N and 30°S, which, due to the spherical form of the planet, represent a huge surface area. Simultaneously, the northern oceans (55–65°N) have, on average, experienced a marked cooling down to 1400 m, and slight warming at greater depths. The southern oceans (55–65°S) have seen slight warming at most depths, but most clearly near the surface. However, averages may be misleading, and quite often better insight is obtained by studying the details (see Section 3).

Sea ice

In 2019, the global sea-ice extent remained well below the average for the satellite era (since 1979), but exhibited stability or a slightly rising trend over the year. At the end of 2016, the global sea-ice extent reached a marked minimum. In the Antarctic, wind conditions played a part, but the global minimum was at least partly caused by the operation of two different natural sea-ice cycles, one in the Northern and one in the Southern Hemisphere. These cycles had simultaneous minima in 2016, with resulting consequences for global sea-ice extent. The minima have now passed, and a trend towards stable or higher ice extent at both poles may have begun during 2019.

Snow cover

Variations in global snow-cover are mainly caused by changes in the Northern Hemisphere, where all the major land areas are located. Southern Hemisphere snow cover is essentially controlled by the Antarctic ice sheet, and is therefore relatively stable. Northern Hemisphere average snow-cover extent has also been stable since the onset of satellite observations, although local and regional interannual variations may be large. Considering seasonal changes since 1979, the Northern Hemisphere snow cover autumn extent is slightly increasing, the mid-winter extent is largely stable, and the spring extent has been slightly decreasing. In 2019, the Northern Hemisphere seasonal snow-cover extent was close to that of the preceding years.

Sea level

Sea level is monitored by satellite altimetry and by direct measurements using tide gauges along coasts. While the satellite-derived record suggests a global sea-level rise of about 3.2 mm per year or more, data from tide gauges along coasts all over the world suggest a stable, average global sea-level rise of less than 1.5 mm per year. Neither of the two types of measurements indicate any modern acceleration in sea-level rise. The marked difference (at least 2:1) between the two datasets still has no broadly accepted explanation, but it is known that satellite observations of sea-level changes are subject to several complications in coastal areas.[1] In addition, for local coastal planning it is only tide-gauge data that is relevant, as will be detailed later in this publication.

Storms and hurricanes

The most recent data on global tropical storm and hurricane accumulated cyclone energy (ACE) is well within the range experienced since 1970. The ACE data series displays considerable variability, but without any clear trend towards higher or lower values. A longer series for the Atlantic Basin (since 1850) suggests a natural cycle of about 60 years' duration in tropical storm and hurricane ACE. In addition, modern data on hurricanes landfalling in the continental USA suggests these remain within the normal range.

2. Atmospheric temperatures

Surface: spatial pattern

The global surface air temperature for 2019 was, on average, somewhat higher than the average of the past ten years. 2017 and 2018 were affected by the aftermath of the major El Niño episode that culminated in early 2016. By 2017, the global surface air temperature was already slowly dropping back towards the pre-2015–16 level, a gradual change that continued throughout 2018, but in 2019 was interrupted by a renewed global surface air temperature increase. The main reason for this change was a new, moderate El Niño episode (see Section 3).

In 2019, Northern Hemisphere surface air temperatures were characterised by regional contrasts, influenced by the dominant jet stream pattern. The most pronounced development was the continuation from 2018 of relatively cold conditions in much of North America. In contrast, most of Europe, Russia, and especially Alaska were relatively warm. Near the Equator, surface air temperatures were generally near the average for the previous 10 years. This was the case in the Southern Hemisphere too, but with a contrast between the oceans, where surface air temperatures were below average, and land areas, where they were above or near average. The relatively low ocean temperature was pronounced in regions between 20°S and 55°S, particularly in the South Atlantic and the Indian Ocean.

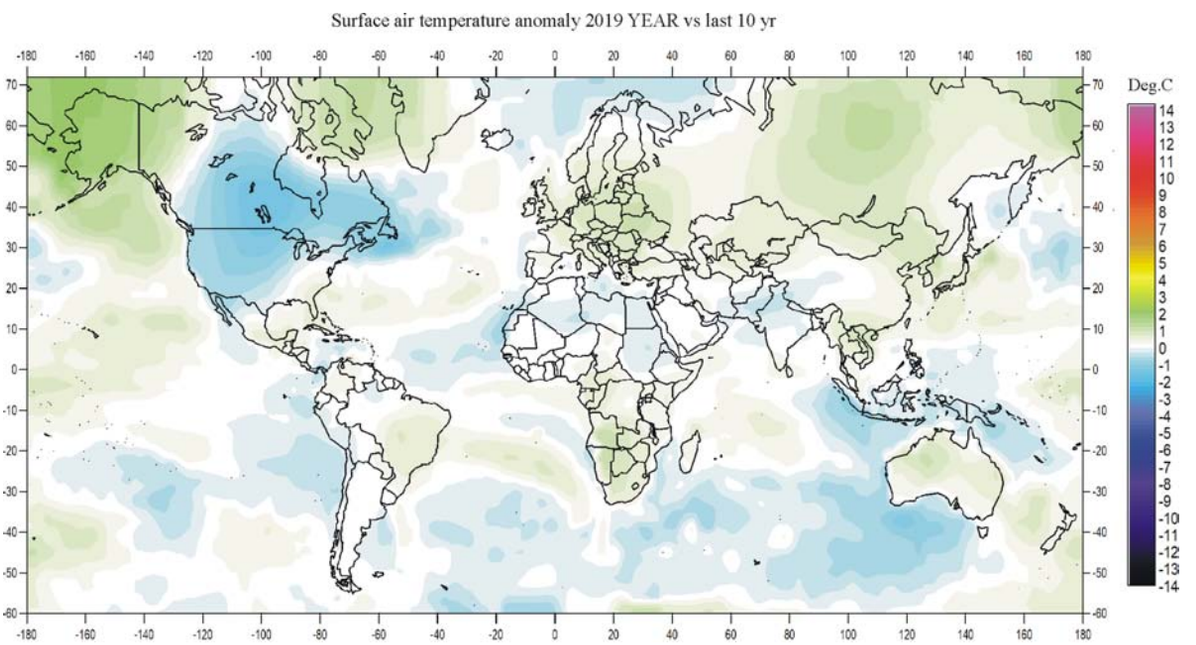

Figure 1: 2019 surface air temperatures compared to the average for the previous 10 years.

Green-yellow-red colours indicate areas with higher temperature than the average, while blue colours indicate lower than average temperatures. Data source: Goddard Institute for Space Studies (GISS) using Hadl_Reyn_v2 ocean surface temperatures, and GHCNv4 land surface temperatures.

In the Arctic, the Baffin Island–West Greenland sector had surface air temperatures above the average of the previous 10 years. The Siberian and Alaskan sectors also had above-average temperatures, in contrast to 2018, when they had been relatively cold. The European sector of the Arctic was relatively cold, although the Arctic temperature record north of 80°N is somewhat implausible, as a result of an interpolation artefact in the record produced by NASA.

The Antarctic was mainly characterised by near-average temperatures in 2019, with no regions being significantly warmer or colder than the average for the past 10 years. A similar interpolation artefact is also in play south of 80°S.

Summing up for 2019, global average air temperatures were higher than during the past 10 years, mainly because of a moderate El Niño. Once again, the dynamics of the equatorial Pacific Ocean have demonstrated their importance for global surface air temperatures, among many other climatic drivers.

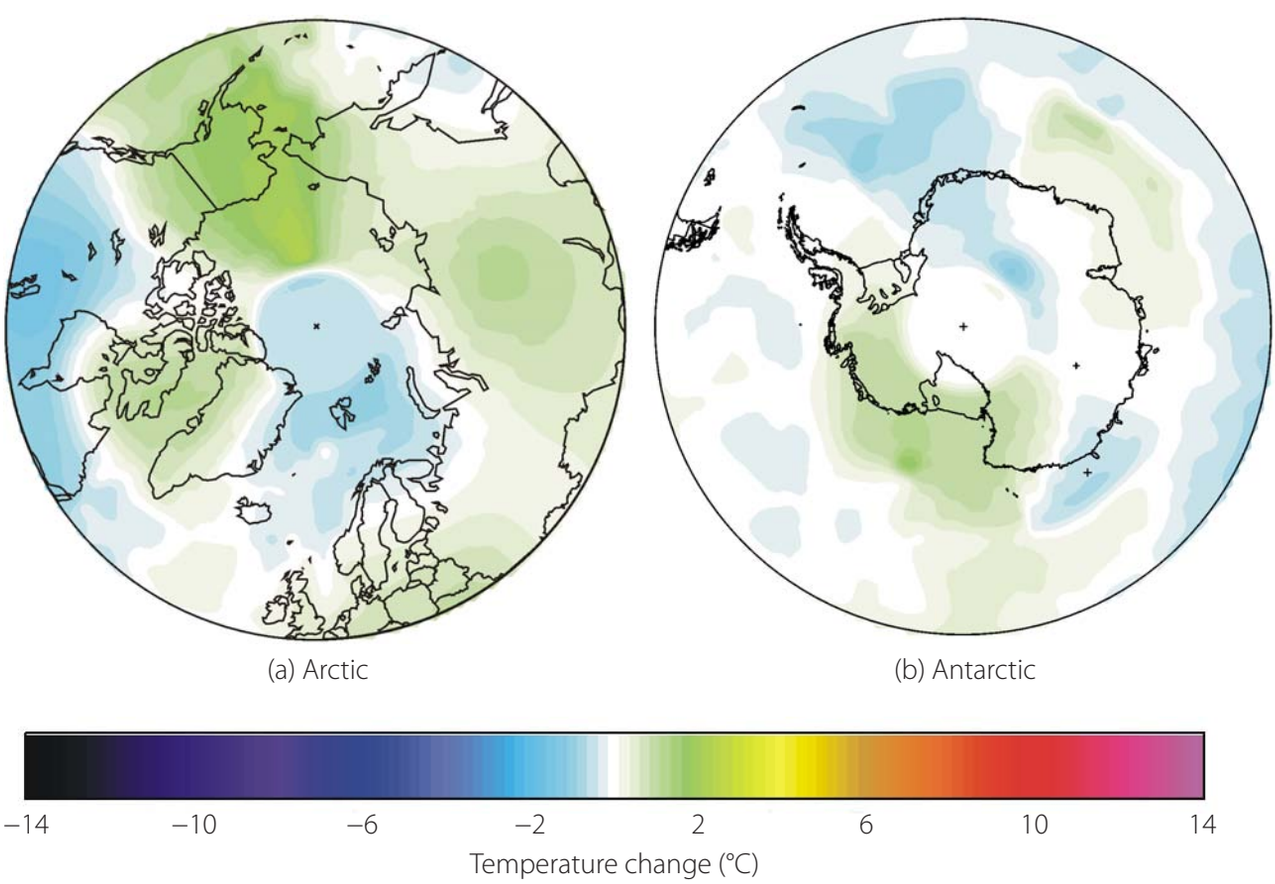

Figure 2: 2019 polar surface air temperatures compared to the average for the previous 10 years.

Green-yellow-red colours indicate areas with higher temperature than the average, while blue colours indicate lower than average temperatures. Data source: Goddard Institute for Space Studies (GISS) using Hadl_Reyn_v2 ocean surface temperatures, and GHCNv4 land surface temperatures.

Lower troposphere: monthly and annual

There are two main temperature records for the lower troposphere, prepared by the University of Alabama, Huntsville (UAH) and Remote Sensing Systems Inc (RSS). Both records clearly show a temperature spike associated with the 2015–16 El Niño, and a subsequent gradual drop, followed by the onset of a new spike due to the moderate 2019 El Niño (Figure 3). The annual means tell the same story (Figure 4)

All temperature series are adjusted as new versions are introduced from time to time. A comparison between the latest (December 2019) record and the May 2015 record (red line in Figure 3) shows that only a few small adjustments have since been made to the UAH series, but that the RSS series has been subject to large adjustments, warming temperatures from 2002 onwards by about +0.1°C. This adjustment of the RSS series was introduced in 2017.

The overall temperature variation in the diagrams (Figure 4) is similar for the two data series, but the overall temperature increase 1979–2019 is larger for RSS than for UAH. Before the 2017 adjustment of the RSS series, the temperature increase was almost identical in the two series.

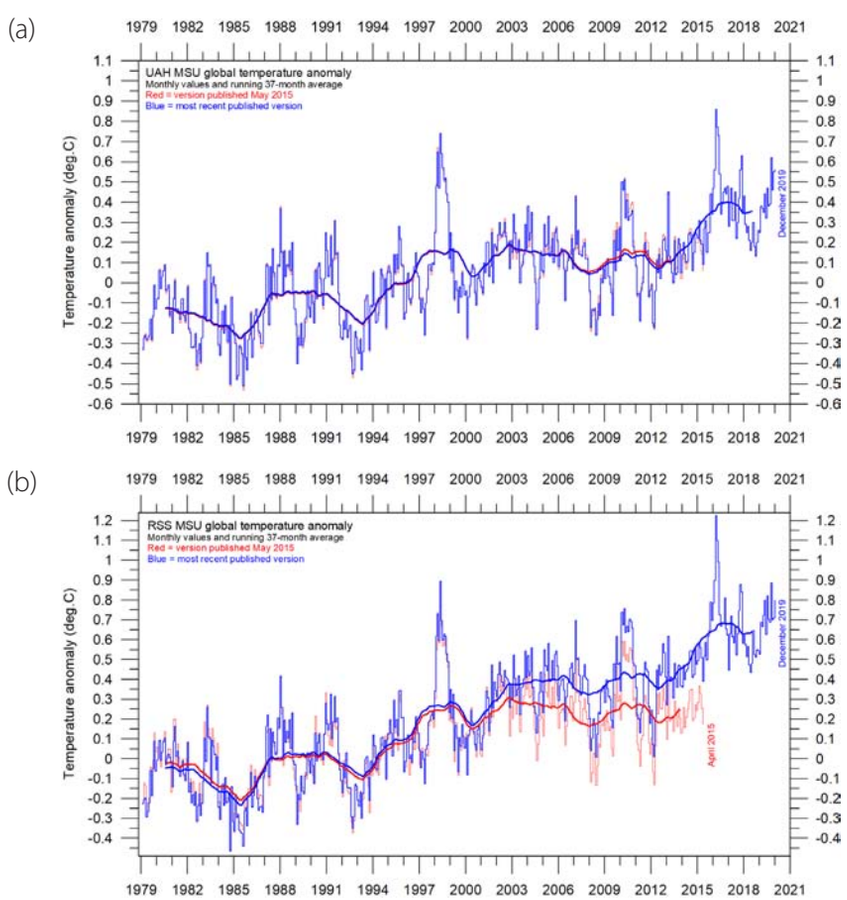

Figure 3: Global monthly average lower troposphere temperatures since 1979.
(a) UAH and (b) RSS. These represent conditions at about 2 km altitude. In each case, the thick line is the simple running 37-month average, nearly corresponding to a running 3-year average.

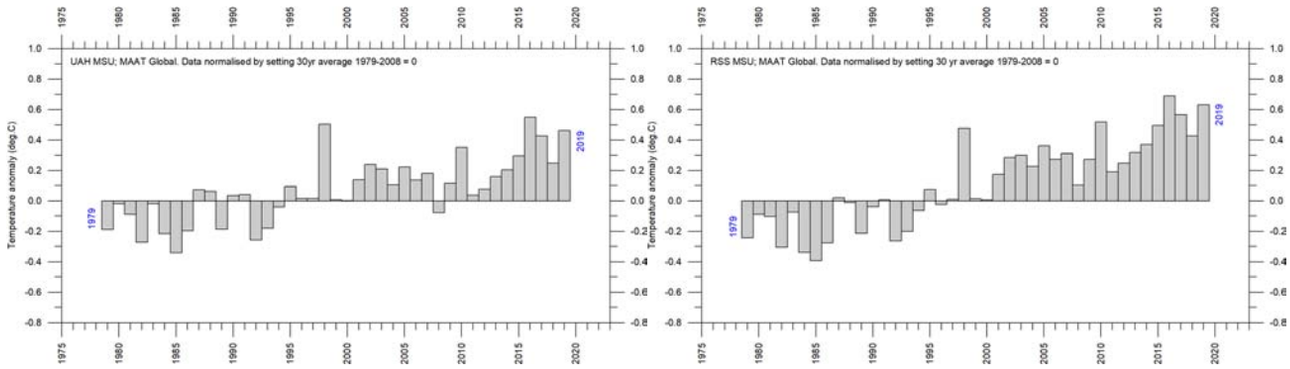

(a) UAH (b) RSS

Figure 4: Global mean annual lower troposphere air temperatures since 1979.

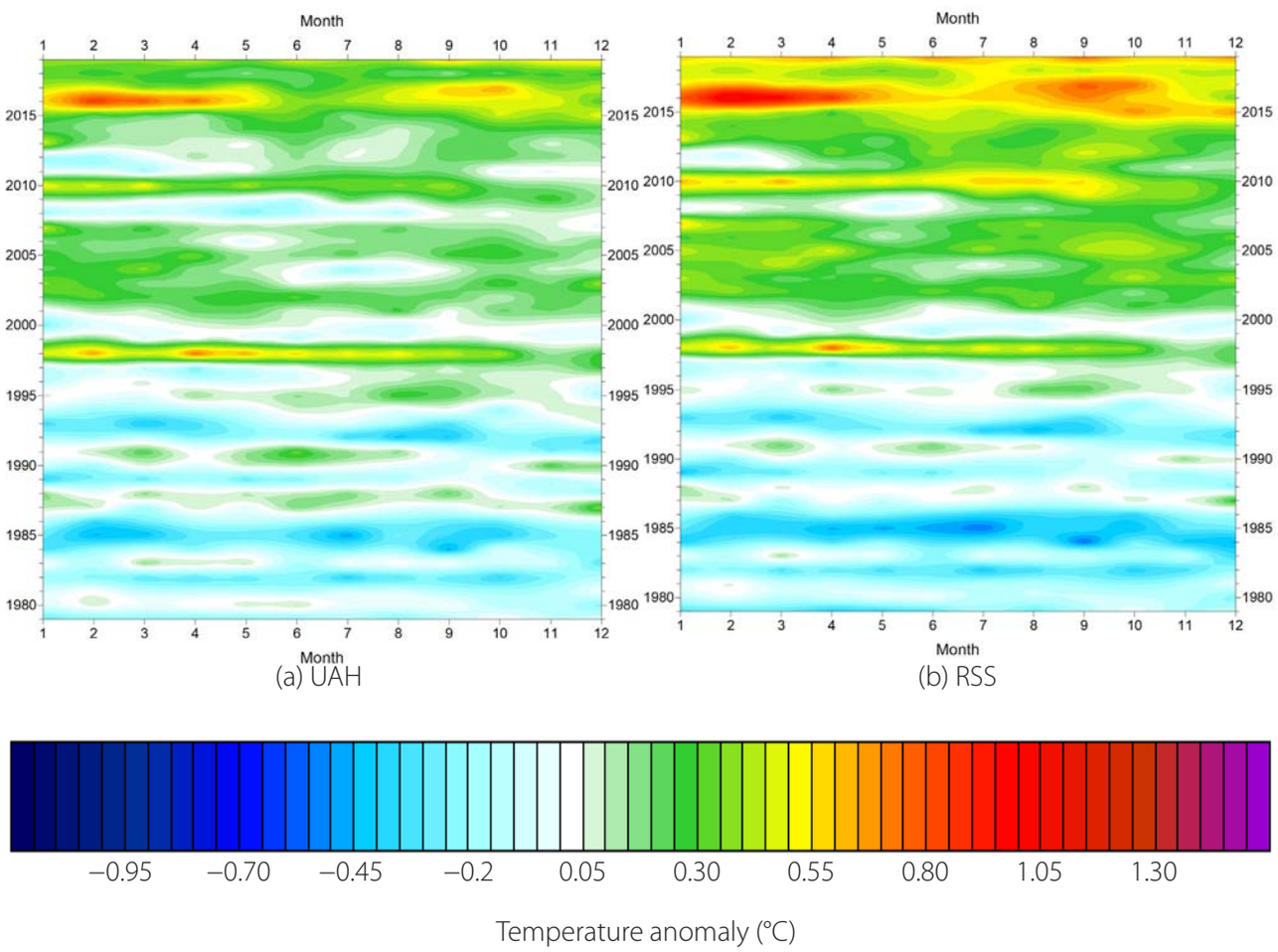

(a) UAH (b) RSS

Figure 5: Temporal evolution of global lower troposphere temperatures since 1979.

Temperature anomaly versus 1979–2008. The effects of the El Niños of 1998, 2010 and 2015–2016 are clearly visible, as are the tendency for many El Niños to culminate during the Northern Hemisphere winter. As the different temperature databases are using different reference periods, the series have been made comparable by setting their individual 30-year average 1979–2008 as zero value.

Surface: monthly

In this paper, I consider three of the available surface temperature records:

- HadCRUT4, a collaborative effort of the Hadley Centre for Climate Prediction and Research and the University of East Anglia's Climatic Research Unit
- NCDC, the record prepared by the US National Climatic Data Center
- GISS, the record prepared by NASA's Goddard Institute for Space Studies.

All three surface air temperature records clearly show the temperature spike associated with the 2015–16 El Niño, the subsequent temperature drop, and the renewed temperature increase due to the moderate 2019 El Niño episode (Figure 6).

The comparison between the most recent (December 2019) record and the May 2015 record (red in Figure 6) shows that few adjustments have been made to the HadCRUT record over that period, while numerous and relatively large changes have been made to both the NCDC and GISS records. All three surface records, however, confirm that the recent major El Niño episode culminated in early 2016, and that there was a subsequent gradual return towards pre-2015 conditions, before a renewed temperature increase in 2019. This development is also shown in Figure 7, which shows the temporal evolution of monthly temperatures.

Figure 6: Global mean annual surface air temperatures since 1979.
(a) HadCRUT4 (b) NCDC (c) GISS.

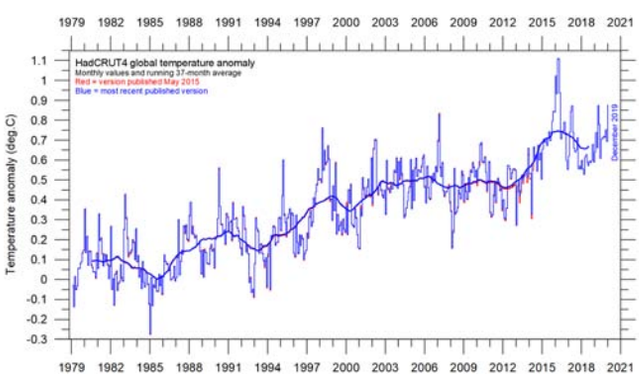

(a) HadCRUT4

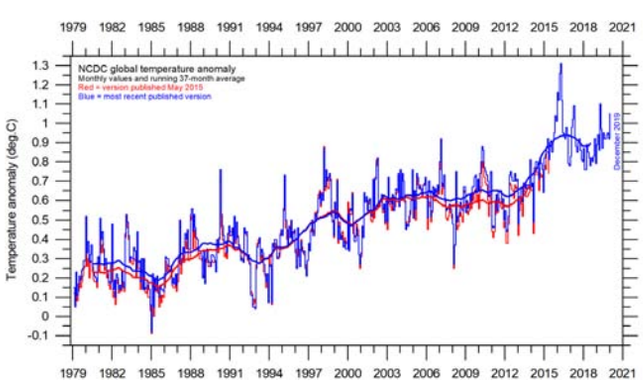

(b) NCDC

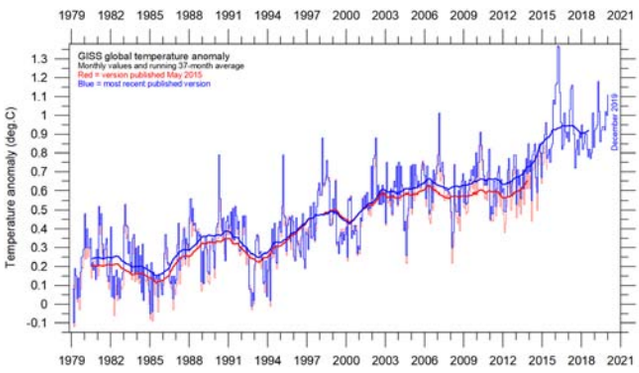

(c) GISS

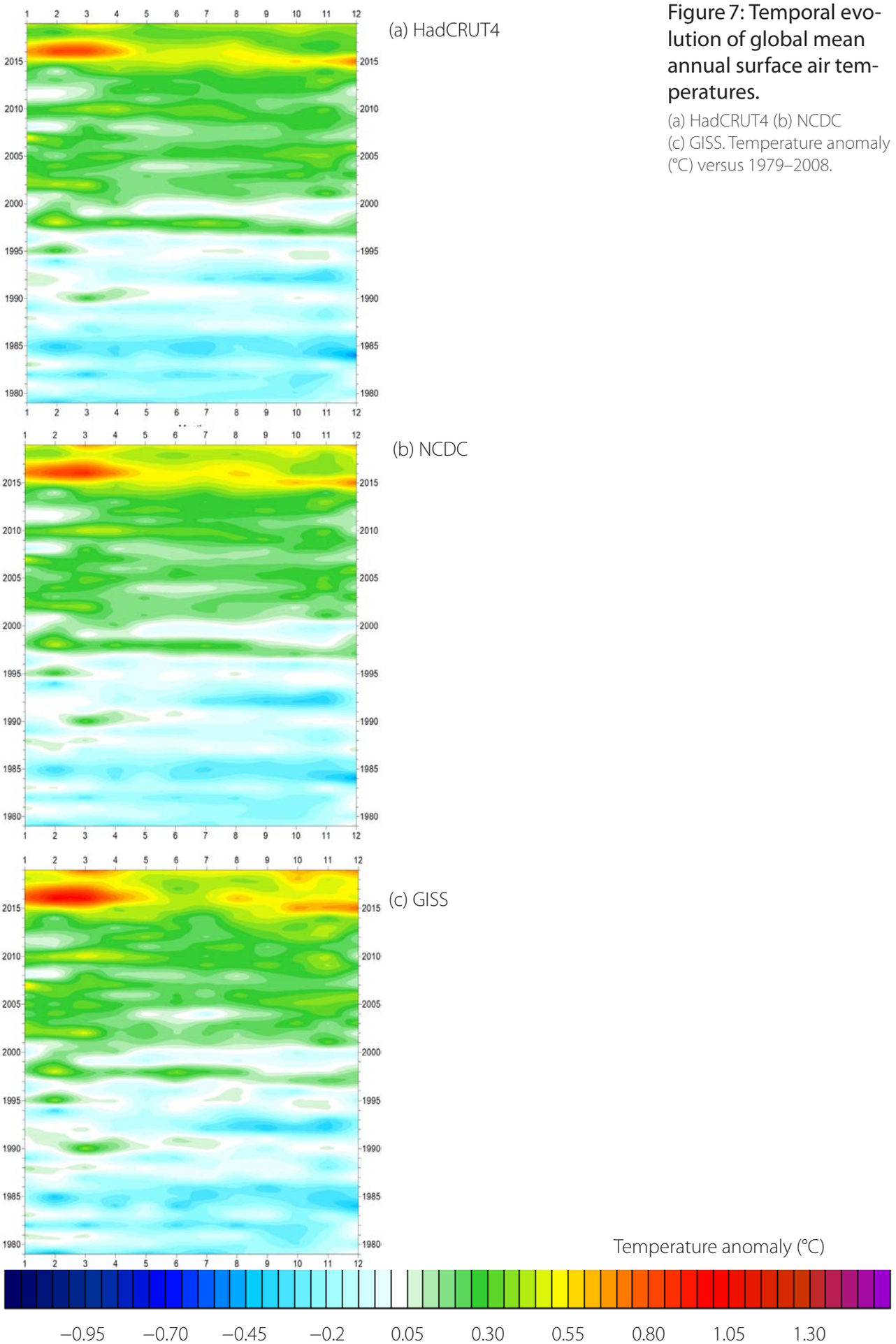

Figure 7: Temporal evolution of global mean annual surface air temperatures.

(a) HadCRUT4 (b) NCDC (c) GISS. Temperature anomaly (°C) versus 1979–2008.

Surface: annual means

All three series show the year 2016 to be the warmest on record, although, as already noted, 2016 saw a strong El Niño episode (Figure 8).

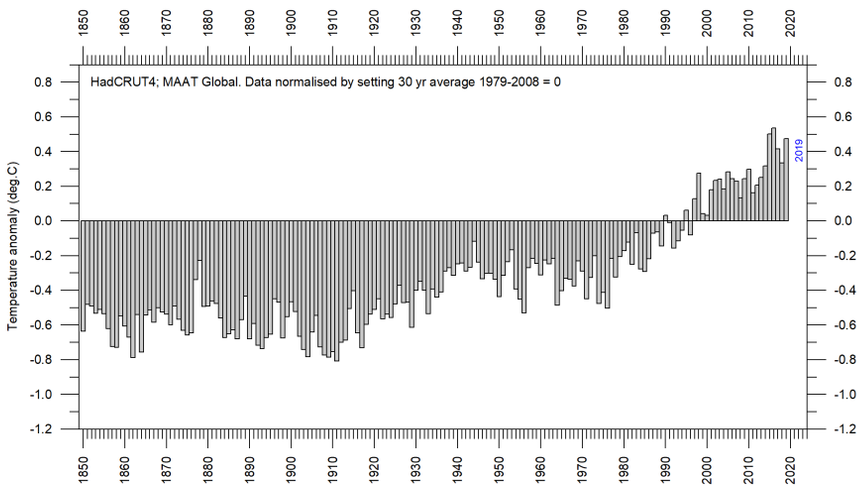

(a) HadCRUT4

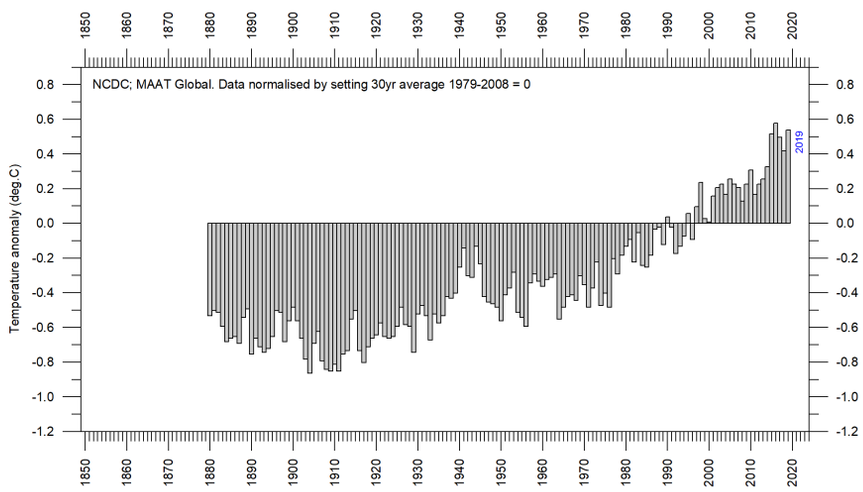

(b) NCDC

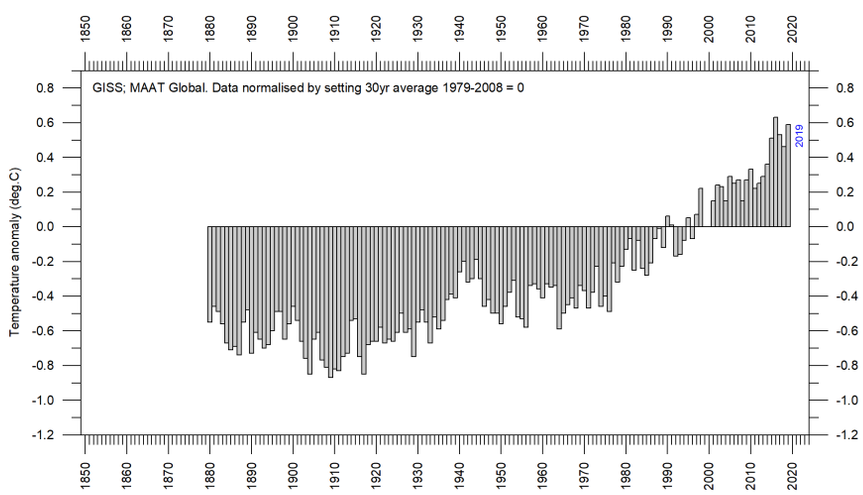

(c) GISS

Figure 8: Global surface air temperatures: annual means.

(a) HadCRUT4 (b) NCDC (c) GISS.

Surface versus lower troposphere

Even though in general there is fair agreement between the different temperature records, there remains a difference between the surface and satellite records, as illustrated in Figure 9. In the early part of the record, the satellite-based temperatures were often somewhat higher than the surface observations. Since 2004, however, the surface records have slowly drifted away from the satellite-based ones, in a warm direction. The major adjustment of the RSS satellite record in 2017 reduced this difference significantly.

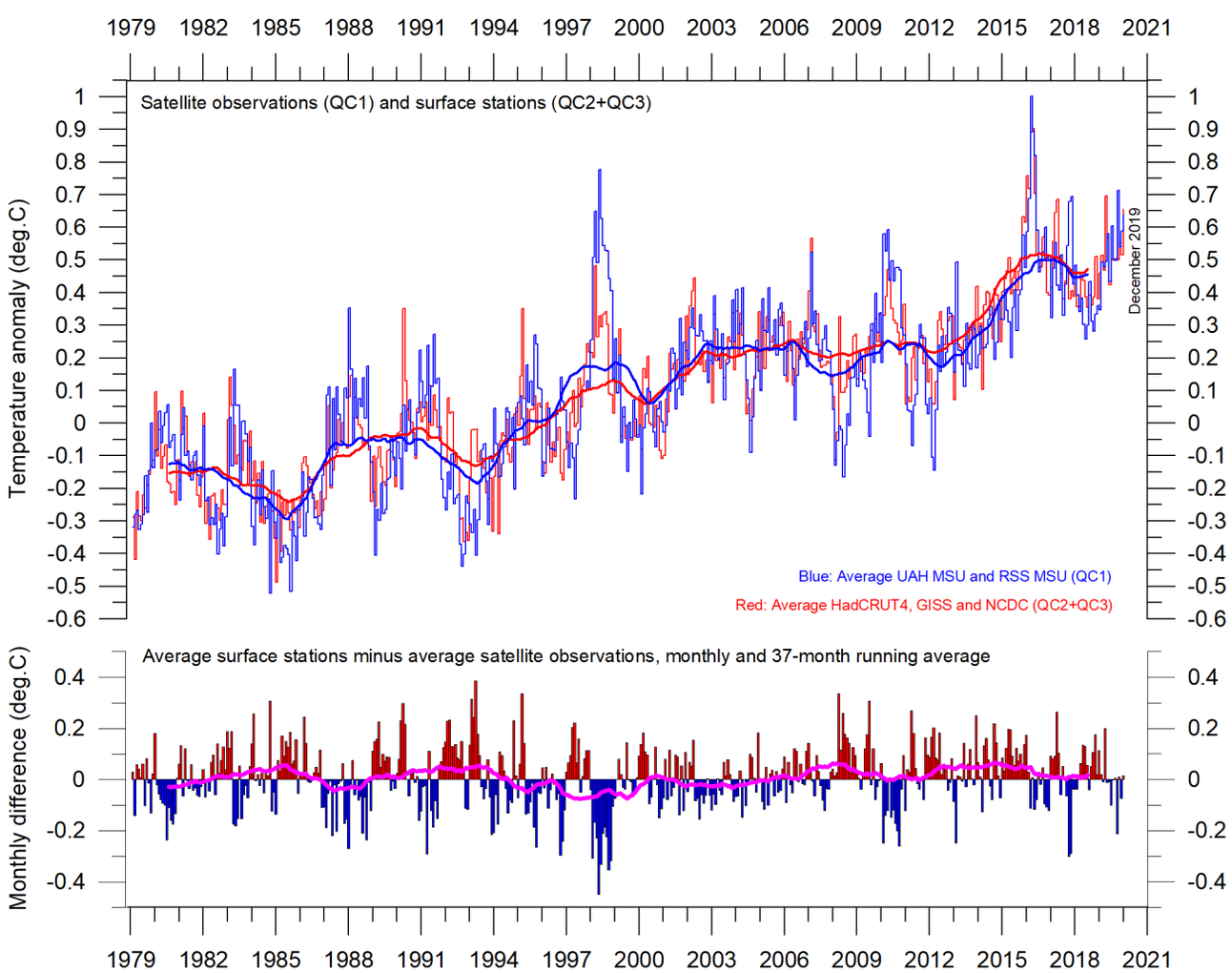

Figure 9: Surface temperatures versus lower troposphere temperatures.

Plot showing the average of monthly global surface air temperature estimates (HadCRUT, NCDC and GISS) and satellite-based lower troposphere temperature estimates (UAH and RSS). The thin lines indicate the monthly value, while the thick lines represent the simple running 37-month average, nearly corresponding to a running 3-year average. The lower panel shows the monthly difference between surface air temperature and satellite temperatures. As the base period differs for the different temperature estimates, they have all been normalised by comparing to the average value of the 30 years from January 1979 to December 2008.

Lower troposphere: over land and ocean

Since 1979, the lower troposphere has warmed much more over land than it has over the oceans (Figure 10). The possible reasons for this difference include variations in incoming solar radiation, cloud cover and land use.

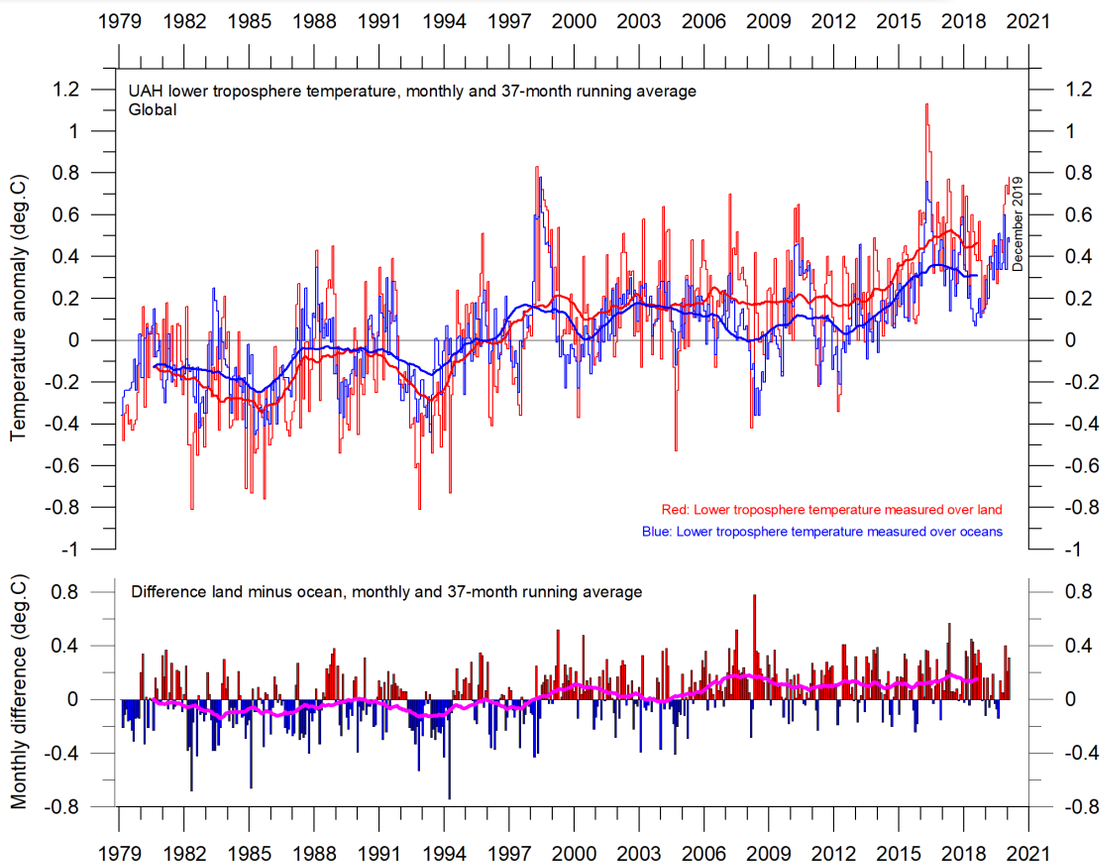

Figure 10: Lower troposphere: over land and ocean.

Global monthly average lower troposphere temperature since 1979 measured over land and oceans, shown in red and blue, respectively, according to University of Alabama at Huntsville (UAH), USA. The thin lines represent the monthly average, and the thick line the simple running 37-month average, nearly corresponding to a running 3-year average.

Upper atmosphere: by altitude

The temperature variations recorded in the lower troposphere are generally reflected at higher altitudes, up to about 10 km (Figure 11). The temperature plateau since about 2002 that is seen in the lower troposphere record is also found at all these altitudes, as is the El Niño induced temperature increase from 2015.

At high altitudes, near the tropopause, the pattern of variations recorded lower in the atmosphere can still be recognised, but for the duration of the record (since 1979) there has been no clear trend towards higher or lower temperatures.

Higher in the atmosphere, in the stratosphere (17 km altitude), two pronounced temperature spikes are visible before the turn of the century. Both of these can be related to major volcanic eruptions as indicated in the diagram. Ignoring these spikes, until about 1995 the stratospheric temperature record shows a persistent decline, ascribed by various scientists to the effect of heat being trapped by carbon di-

oxide in the troposphere below. However, the marked stratospheric temperature decline essentially ends around 1995–96, since when there has been a long temperature plateau. Thus the stratospheric temperature 'pause' began 5–7 years before the start of the similar 'pause' in the lower troposphere. Since 2015, roughly in concert with the El Niño induced tropospheric temperature increase, a small temperature decrease has taken place in the stratosphere.

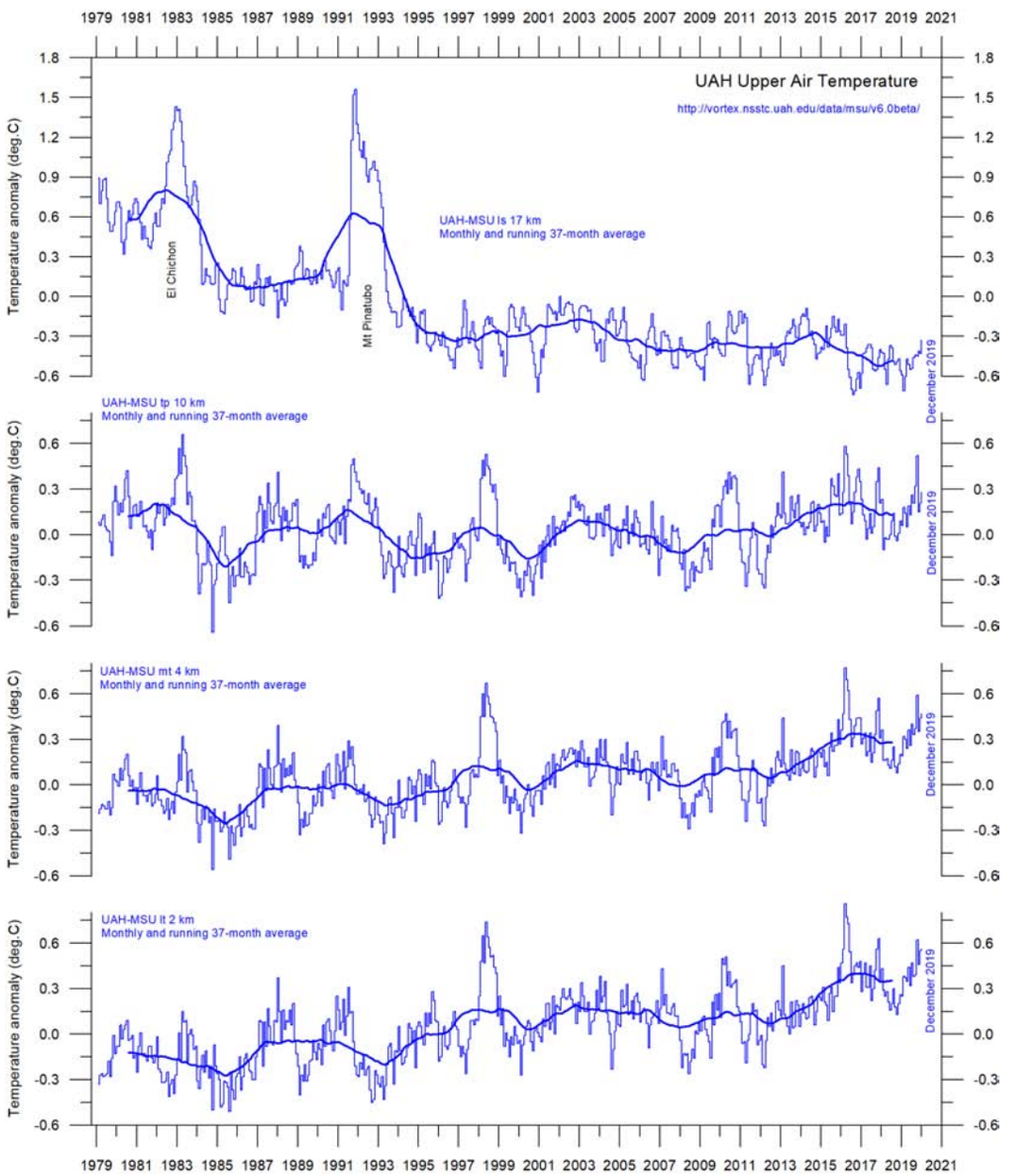

Figure 11: Temperatures by altitude.

Global monthly average temperature in different altitudes according to University of Alabama at Huntsville (UAH), USA. The thin lines represent the monthly average, and the thick lines the simple running 37-month average, nearly corresponding to a running 3-year average.

Atmospheric greenhouse gases

Water vapour is the most important greenhouse gas in the troposphere. The highest concentration is found within a latitudinal range from 50°N to 60°S. The two polar regions of the troposphere are comparatively dry.

Figure 12 shows the specific atmospheric humidity to be stable or slightly increasing up to about 4–5 km altitude. At higher levels in the troposphere (about 9 km), the specific humidity has been decreasing for the duration of the record (since 1948), but with shorter variations superimposed on the falling trend. A Fourier frequency analysis (not shown here) shows these variations to be particularly influenced by a periodic variation of about 3.7 years' duration.

The persistent decrease in specific humidity at about 9 km altitude is noteworthy, as this altitude roughly corresponds to the level at which the theoretical temperature effect of increased atmospheric carbon dioxide is expected initially to play out.

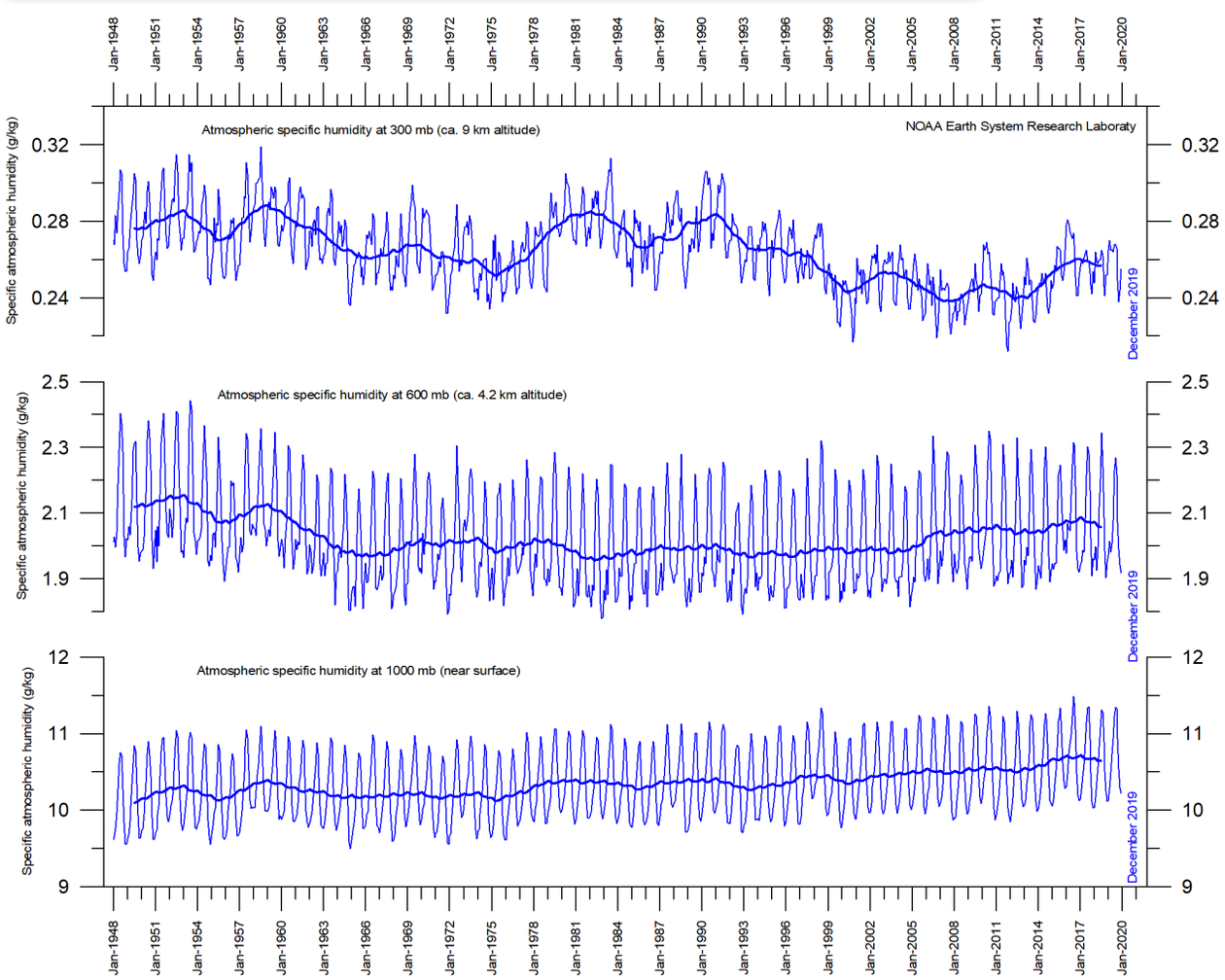

Figure 12: Humidity.

Specific atmospheric humidity (g/kg) at three different altitudes in the troposphere since January 1948. The thin lines show monthly values, while the thick lines show the running 37-month average (about 3 years). Data source: Earth System Research Laboratory (NOAA).

Carbon dioxide (CO_2) is an important greenhouse gas, although less important than water. For the duration of the record (since 1958), an increasing trend is clearly visible, with an annual cycle superimposed. At the end of 2019, the amount of atmospheric CO_2 was close to 410 ppm (Figure 13). Carbon dioxide is usually considered a relatively well-mixed gas in the troposphere.

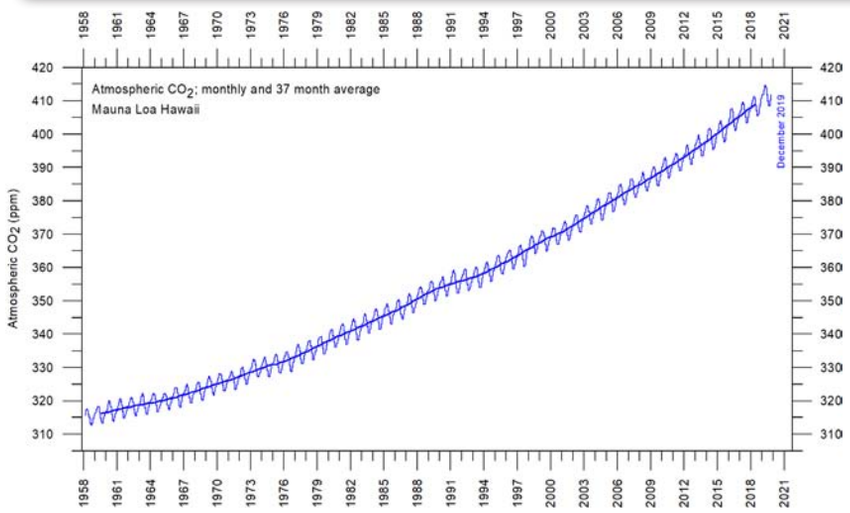

Figure 13: CO_2 concentration.
Monthly amount of atmospheric CO_2 since March 1958, measured at the Mauna Loa Observatory, Hawaii. The thin line shows the monthly values, while the thick line is the simple running 37-month average, nearly corresponding to a running 3-year average.

The annual change in tropospheric CO_2 has been increasing, from about +1 part per million (ppm) per year in the early part of the record to more than 2.5 ppm/year towards the end of the record (Figure 14). A Fourier frequency analysis (not shown here) shows the annual change of tropospheric CO_2 to be influenced by periodic variations of 2.5- and 3.8-years' duration.

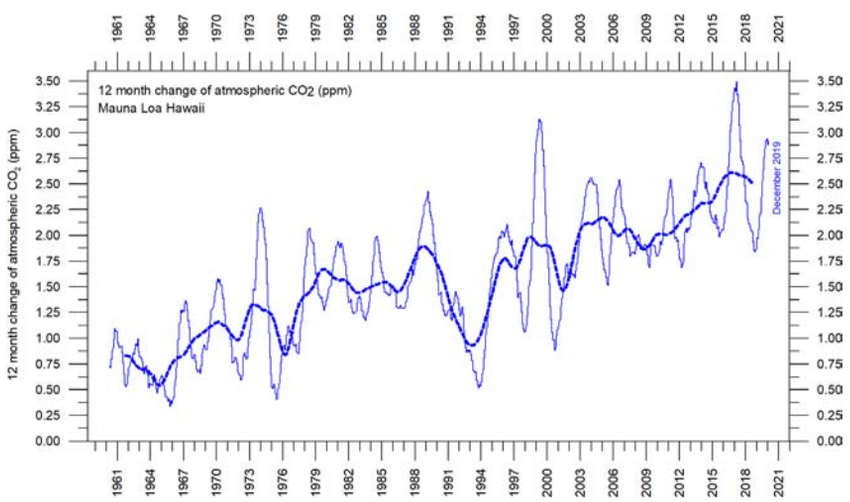

Figure 14: Growth in CO_2 concentration.
Annual (12-month) growth rate (ppm) of atmospheric CO_2 since 1959, calculated as the average amount of atmospheric CO_2 during the last 12 months, minus the average for the preceding 12 months. The graph is based on data measured at the Mauna Loa Observatory, Hawaii. The thin blue line shows the value calculated month by month, while the dotted blue line represents the simple running 3-year average.

It is instructive to consider the variation of the annual change rate of atmospheric CO_2 together with the annual change rates for global air and sea surface temperatures (Figure 15). All three change rates clearly vary in concert, but with sea surface temperatures leading – a few months ahead of the global temperature and 11–12 months ahead of the change rates for atmospheric CO_2.

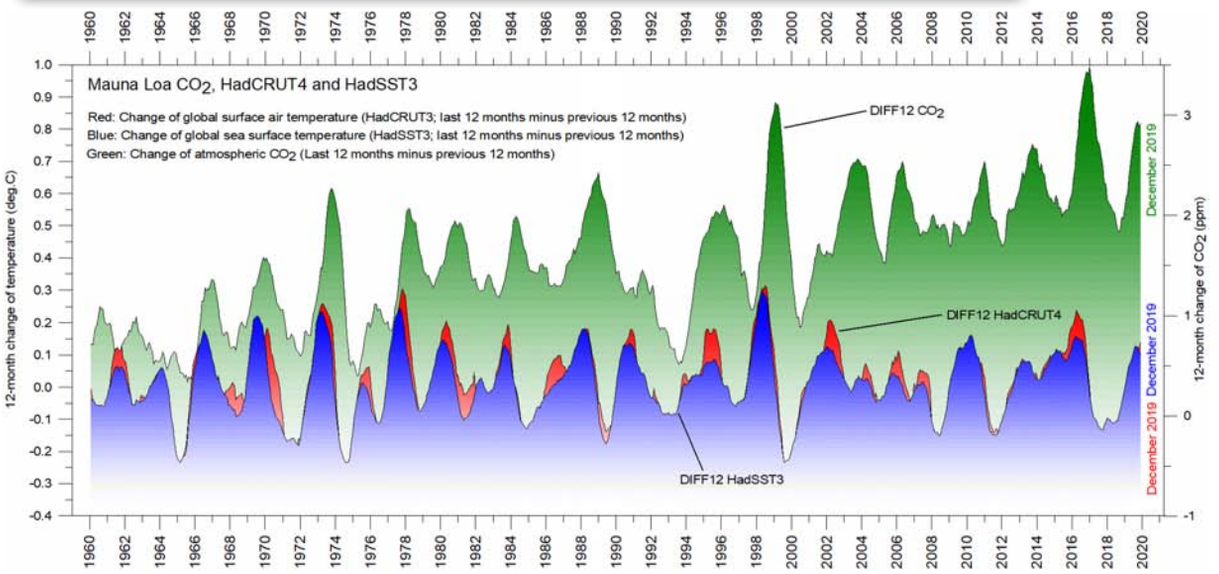

Figure 15: CO_2 versus temperature.

Annual (12-month) change of global atmospheric CO2 concentration (Mauna Loa; green), global sea surface temperature (HadSST3; blue) and global surface air temperature (HadCRUT4; red). All graphs are showing monthly values of DIFF12, the difference between the average of the last 12 months and the average for the previous 12 months for each data series.

Figure 16 shows the visual association between the annual change of atmospheric CO_2 and La Niña and El Niño episodes, emphasising the importance of oceanographic dynamics for understanding changes in atmospheric CO_2.

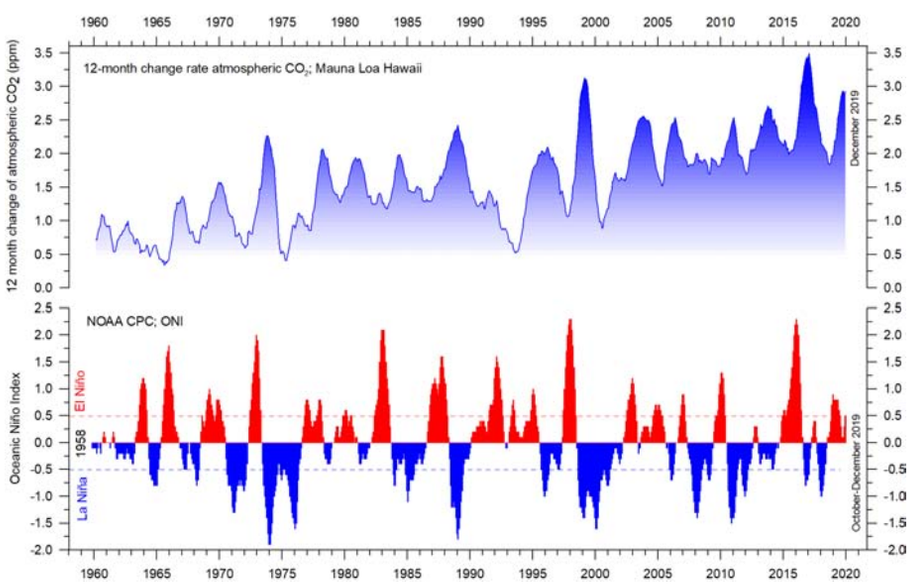

Figure 16: CO_2 and El Niño.

Visual association between annual growth rate of atmospheric CO_2 (upper panel) and the Oceanic Niño Index (lower panel). See also Figures 14 and 15).

Lower troposphere: by latitude

Figure 17 shows that the 'global' warming experienced after 1980 has predominantly been a Northern Hemisphere phenomenon, and that it mainly played out as a marked change between 1994 and 1999. This apparently rapid temperature change was, however, influenced by the Mt. Pinatubo eruption of 1992–93 and the subsequent 1997 El Niño episode.

The figure also reveals how the temperature effects of equatorial El Niños – strong ones in 1997 and 2015–16 and the moderate one in 2019 – apparently spread to higher latitudes in both hemispheres, although with some delay. This El Niño temperature effect was mainly seen in the Northern Hemisphere.

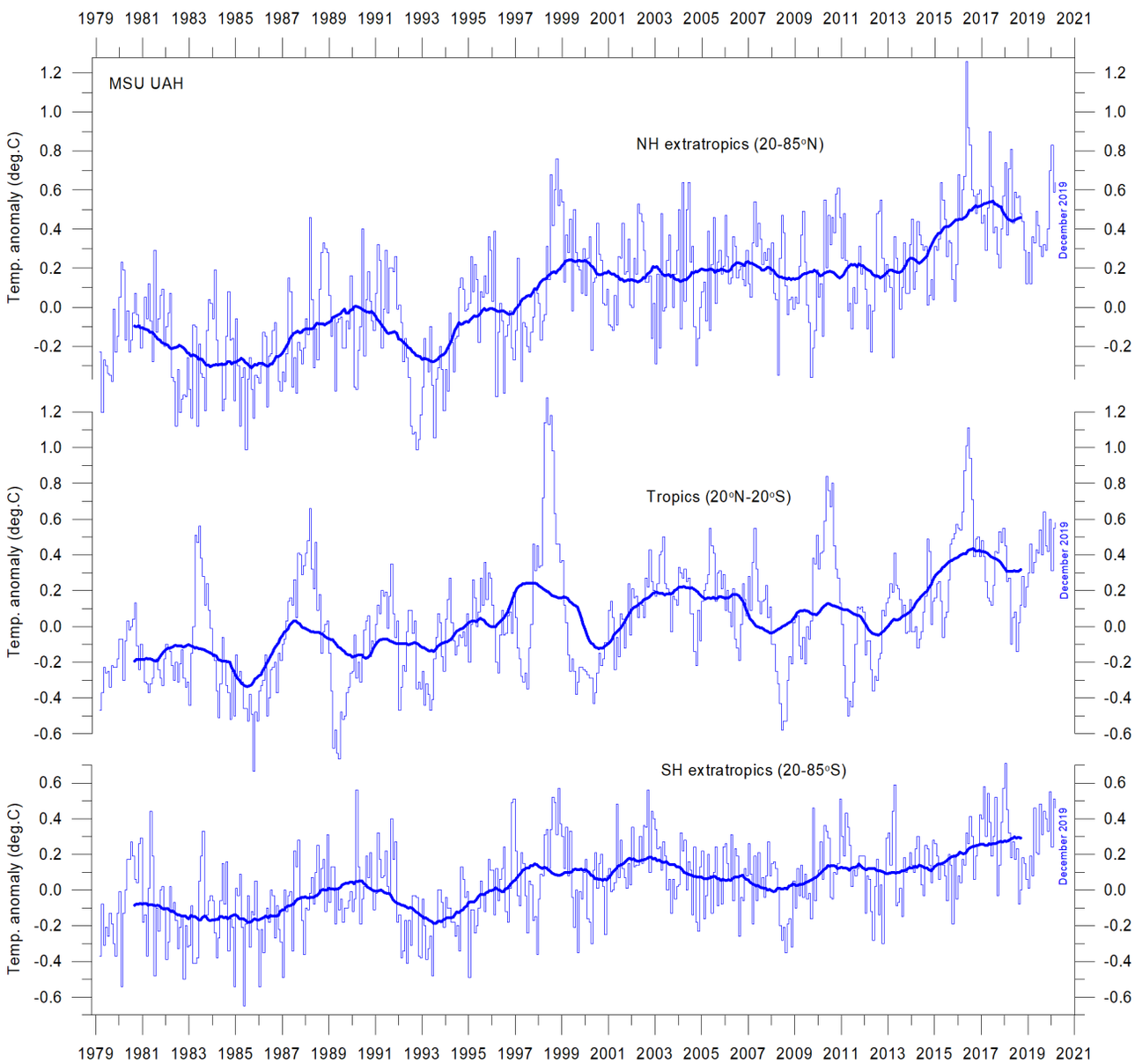

Figure 17: Zonal air temperatures

Global monthly average lower troposphere temperature since 1979 for the tropics and the northern and southern extratropics, according to UAH. Thick lines are the simple running 37-month average, nearly corresponding to a running 3-year average.

Lower troposphere: polar

In the Arctic, warming mainly took place between 1994 and 1996, and less so subsequently (Figure 18). In 2016, however, temperatures peaked for several months, presumably because of oceanic heat emitted to the atmosphere during the 2015–16 El Niño (see also Figure 16) and then advected to higher latitudes. A temperature decrease has characterised the Arctic since 2016.

In the Antarctic, temperatures have remained almost stable since the onset of the satellite record in 1979. In 2016–17, a small temperature peak is visible in the monthly record. This may be interpreted as the subdued effect of the recent El Niño episode.

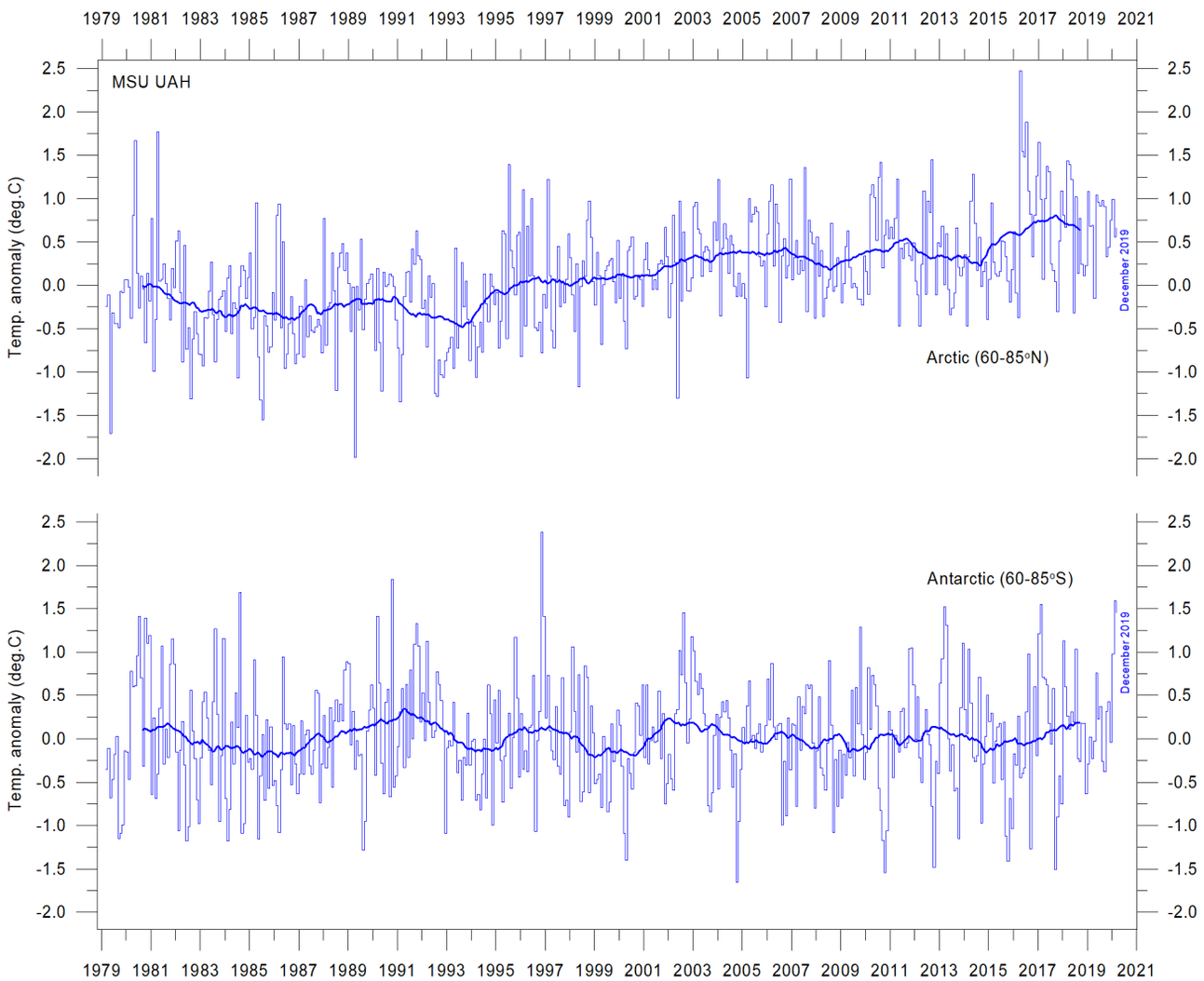

Figure 18: Tropospheric temperatures above the poles.

Global monthly average lower troposphere temperature since 1979 for the North Pole and South Pole regions, according to UAH. Thick lines are the simple running 37-month average, nearly corresponding to a running 3-year average.

3. Ocean temperatures

Surface: spatial patterns in recent years

Figure 19 shows the spatial patterns of ocean temperatures for December 2017, 2018 and 2019. December 2017 was a weak La Niña episode, December 2018 was approximately neutral, as was December 2019, following the moderate El Niño characterising most of that year.

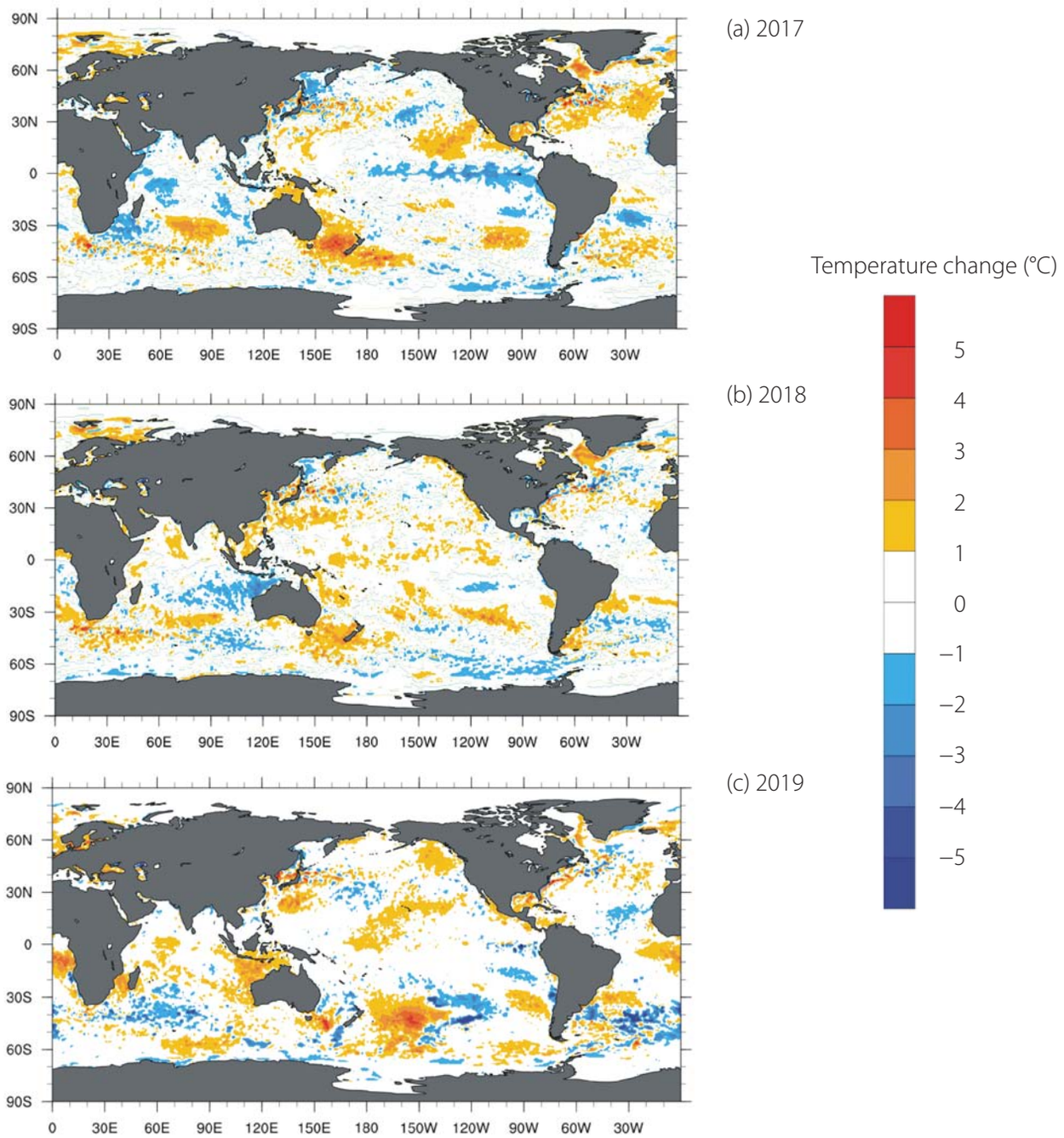

Figure 19: Spatial patterns of ocean surface temperatues, 2017–2019.

Sea surface temperature anomalies at the end of December 2017, 2018 and 2019, respectively. The maps show the current anomaly (deviation from normal) of the surface temperature of Earth's oceans. Reference period: 1977–1991. Dark grey represents land areas. Map source: Plymouth State Weather Center.

Figure 20 shows all El Niño and La Niña episodes since 1950. The 2015–16 El Niño is among the strongest recorded. Considering the entire record, however, recent variations between El Niño and La Niña episodes do not appear abnormal in any way.

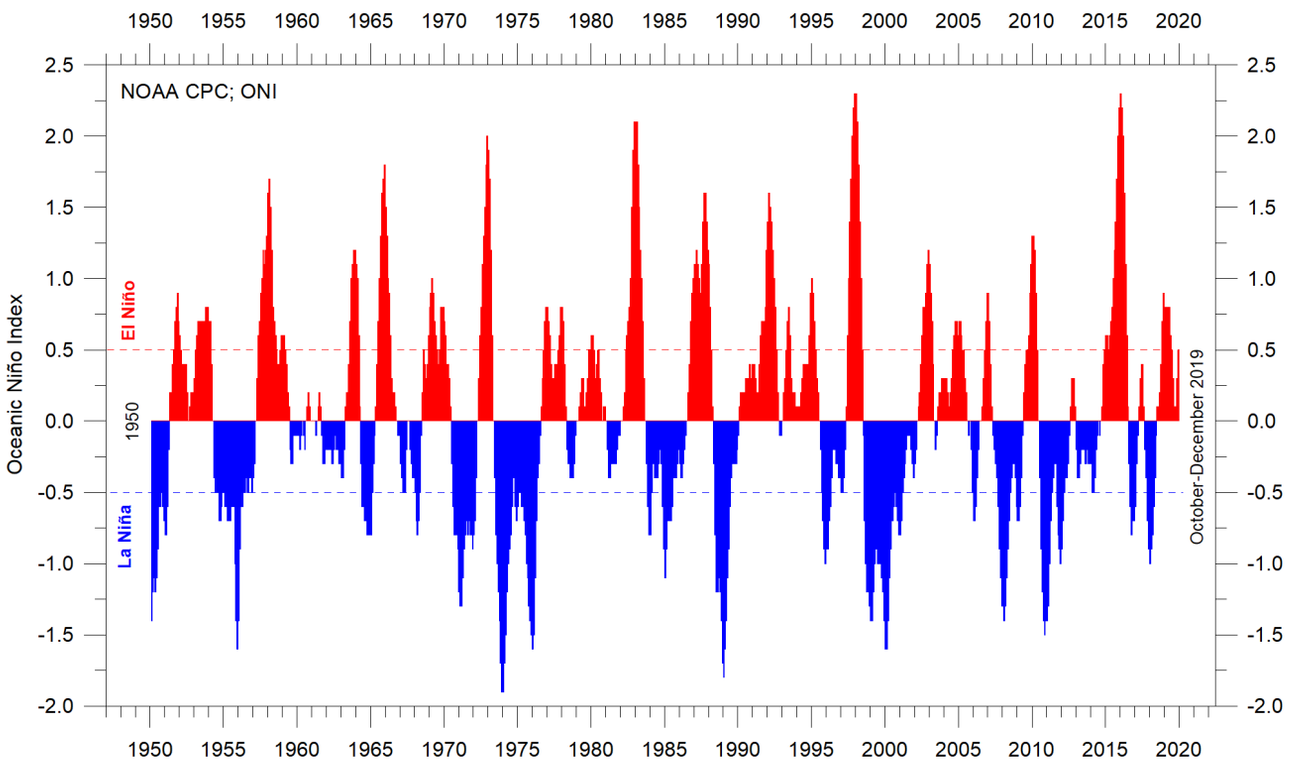

Figure 20: Warm and cold episodes on the Oceanic Niño Index.

Warm and cold episodes for the Oceanic Niño Index, defined as 3-month running mean of ERSSTv4 SST anomalies in the Niño 3.4 region (5°N–5°S, 120°–170°W). Anomalies are centred on 30-year base periods updated every 5 years.

Average temperature to 1900 m depth, by region

Based on observations by Argo floats,[2] Figure 21 shows that, on average, the temperature of the global oceans down to 1900 m depth has been increasing since about 2011. It also shows that since 2013 this increase has mostly been manifested in changes near the Equator, between 30°N and 30°S. In contrast, for the circum-Arctic oceans north of 55°N, depth-integrated ocean temperatures have been decreasing since 2011. Near the Antarctic, south of 55°S, temperatures have essentially been stable. At most latitudes, a clear annual rhythm is seen.

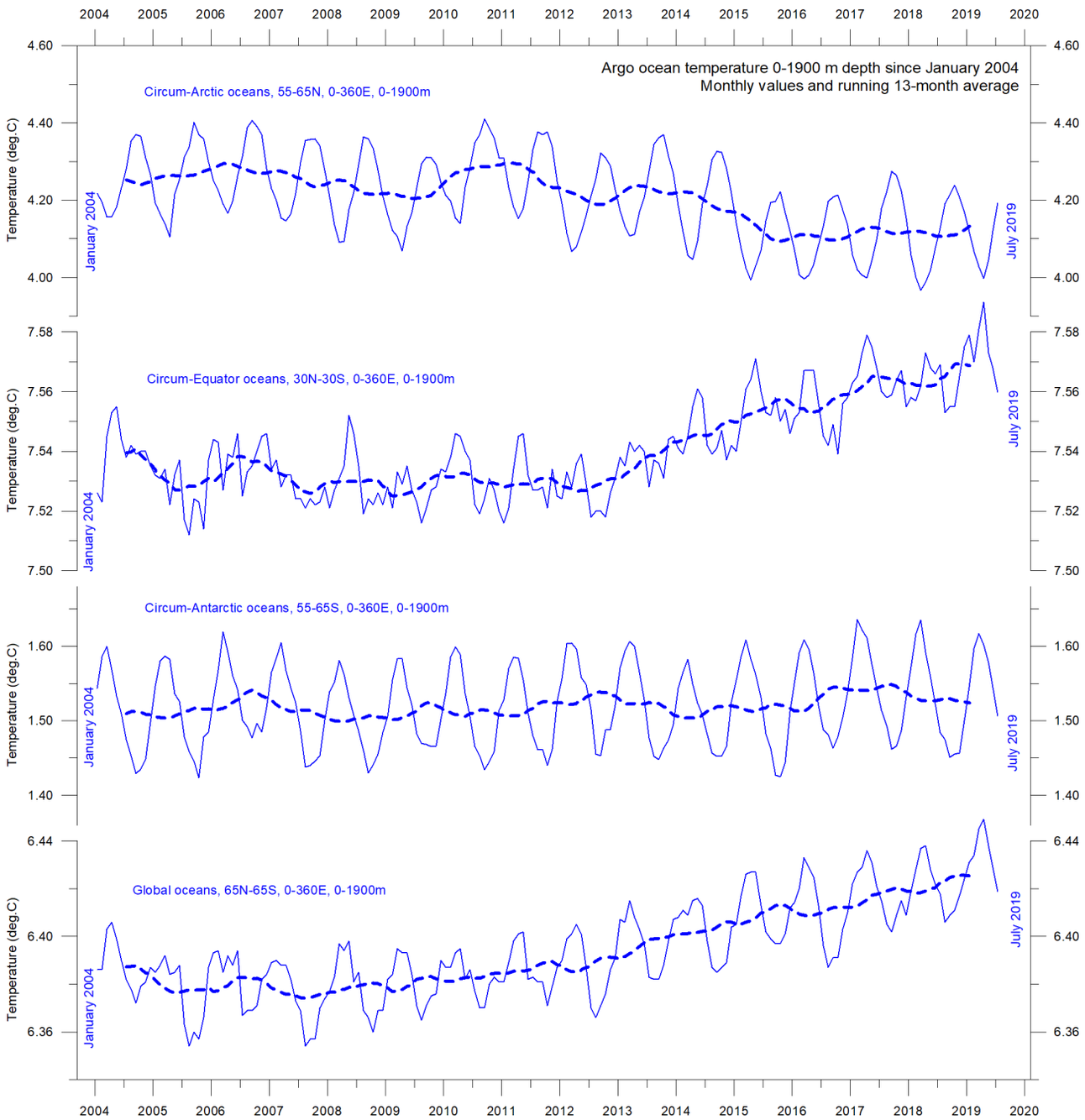

Figure 21: Average ocean temperatures in selected latitudinal bands.

Average ocean temperatures January 2004–July 2029 at 0–1900 m depth in selected latitudinal bands The thin line shows monthly values and the thick stippled line shows the running 13-month average. Source: Global Marine Argo Atlas..

Global average: by depth

Figure 22 shows global average ocean temperatures at different depths. An annual rhythm can be seen, down to about 100 m depth. In the uppermost 100 m, temperatures have increased since about 2011. For 200–400 m depth, temperatures have exhibited little change during the observation period.

For depths below 400 m, however, temperatures are again seen to be increasing. Interestingly, the diagram suggests that this increase first began at 1900 m depth around 2009, and from there gradually spread upwards. At 600 m depth, the temperature increase began in around 2012; that is, about three years after it was seen at 1900 m. The timing of these changes shows that average temperatures in the upper 1900 m of the oceans are not only influenced by conditions playing out at or near the ocean surface, but also by processes operating at greater depths than 1900 m.

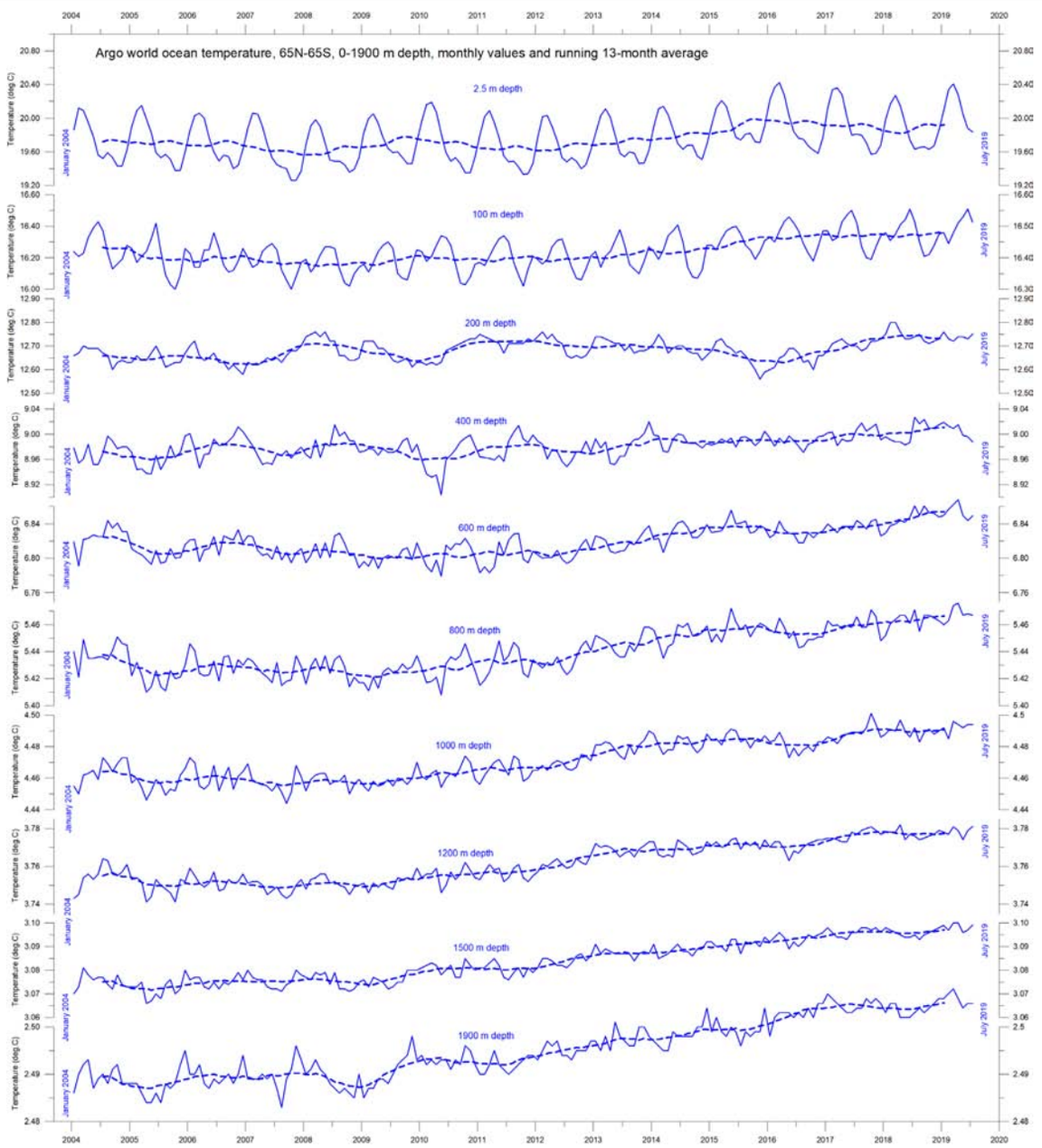

Figure 22: Global Ocean temperatures at different depths.

Global ocean temperatures January 2004–July 2019 at different depths between 65°N and 65°S. The thin line shows monthly values and the stippled line shows the running 13-month average. Source: Global Marine Argo Atlas.

Thus part of the present ocean warming appears to be due to circulation features operating in the depths of the oceans; they are not directly related to processes operating at or near the surface.

This can also be seen in Figure 23, which shows the net change of global ocean temperatures at different depths, calculated as the difference between the 12-month averages for January–December 2004 and August 2018–July 2019, respectively. The largest net changes occurred in the uppermost 200 m. However, average values, as shown in this diagram, although valuable, also hide many interesting regional details, as shown in Figure 24.

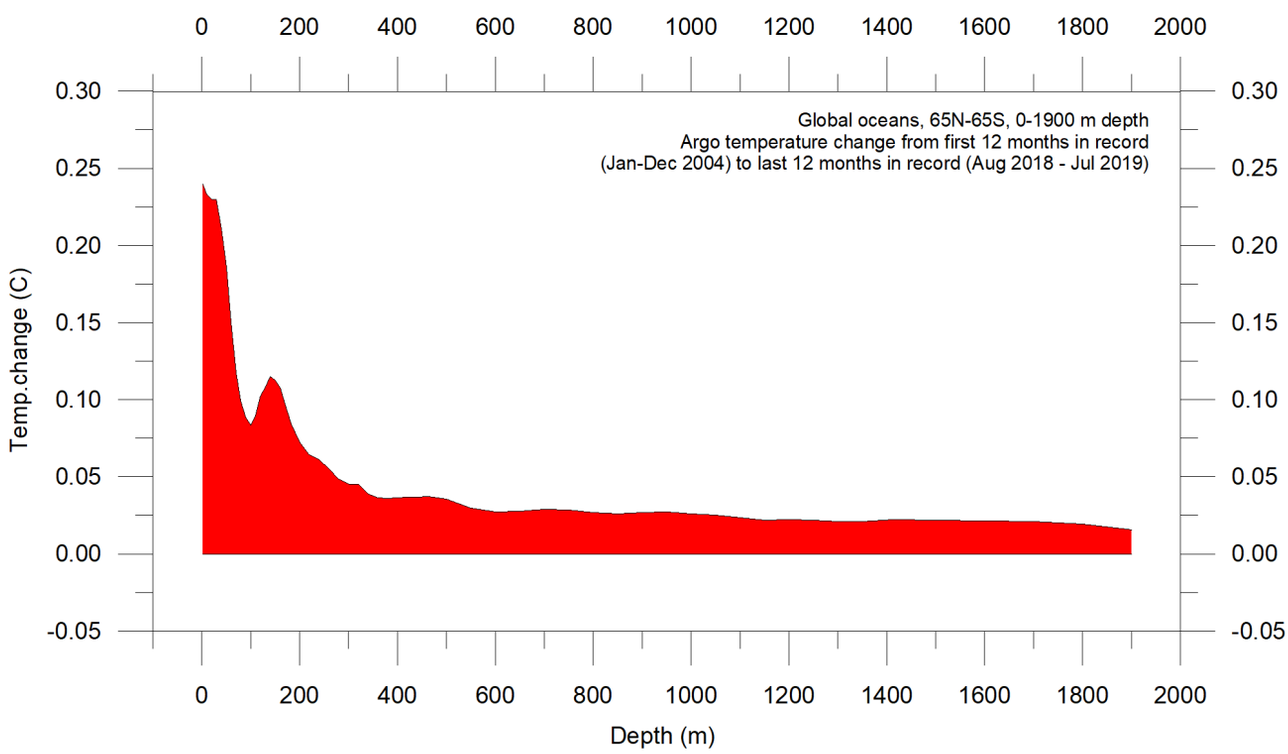

Figure 23: Global ocean net temperature change since 2004 from surface to 1900 m depth.
Source: Global Marine Argo Atlas.

Regional, 0–1900 m depth: changes 2004–2019

Figure 24 shows the latitudinal variation of ocean temperatures net changes, January–December 2004 versus August 2018–July 2019, for various depths, calculated as in the previous diagram. The three panels show the net change for the Arctic oceans (55–65°N), equatorial oceans (30N–30°S), and Antarctic oceans (55–65°S), respectively.

The global surface net warming shown in Figure 23 affects the equatorial and Antarctic oceans, but not the Arctic oceans (Figure 24). In fact, net cooling is pronounced down to 1400 m depth for the northern oceans. However, the major part of Earth's land areas is in the Northern Hemisphere, so the surface area (and volume) of Arctic oceans is much smaller than that of the Antarctic

oceans, which in turn is smaller than the equatorial oceans. In fact, half of the planet's surface area (land and ocean) is located between 30°N and 30°S.

Nevertheless, the contrast in net temperature change over 2004–2019 for the different latitudinal bands is instructive. For the two polar oceans, the Argo data appears to demonstrate the existence of a bi-polar seesaw, a phenomenon that was described by Chylek et al. in 2010. It is no less interesting that the near-surface ocean temperatures in the two polar oceans contrasts with the trends in sea ice in the two polar regions (see Section 6).

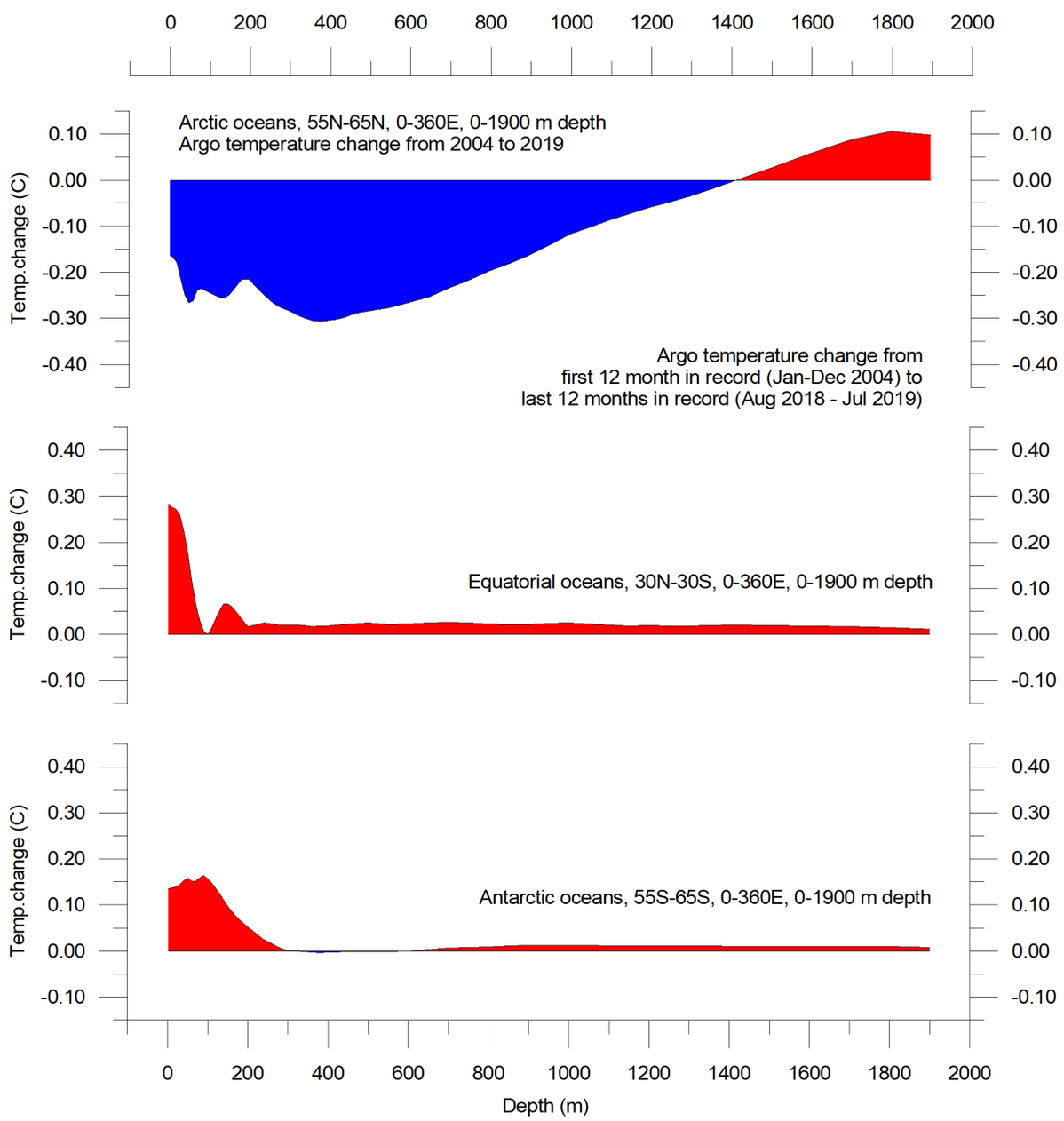

Figure 24: Net temperature change since 2004 from surface to 1900 m depth in different parts of the global oceans, using Argo data.

Source: Global Marine Argo Atlas.

Change 2004–2019 in selected sectors

In this section, I consider net temperature changes for the period 2004–2018/19 along two north–south transects, one along 20°W, representing the Atlantic Ocean, and the other along 150°W, representing the Pacific. (In passing, I also look at a short east-west transect, representing the North Atlantic Current.) The locations of the transects are shown in Figure 25, and the temperature changes in Figures 26–28. To prepare the latter, 12-month average ocean temperatures for January–December 2018 and August 2018 – July 2019 were compared to annual average temperatures for 2004, representing the initial 12 months in the Argo-record. To give an insight into the most recent changes, the net change in 12-month average temperatures is shown for both 2004–2018 (on top) and 2004–2018/19. Warm colours indicate net warming from 2004 to 2018/19, and blue colours cooling. Due to the spherical shape of the Earth, northern and southern latitudes represent only small ocean volumes compared to latitudes near the Equator.

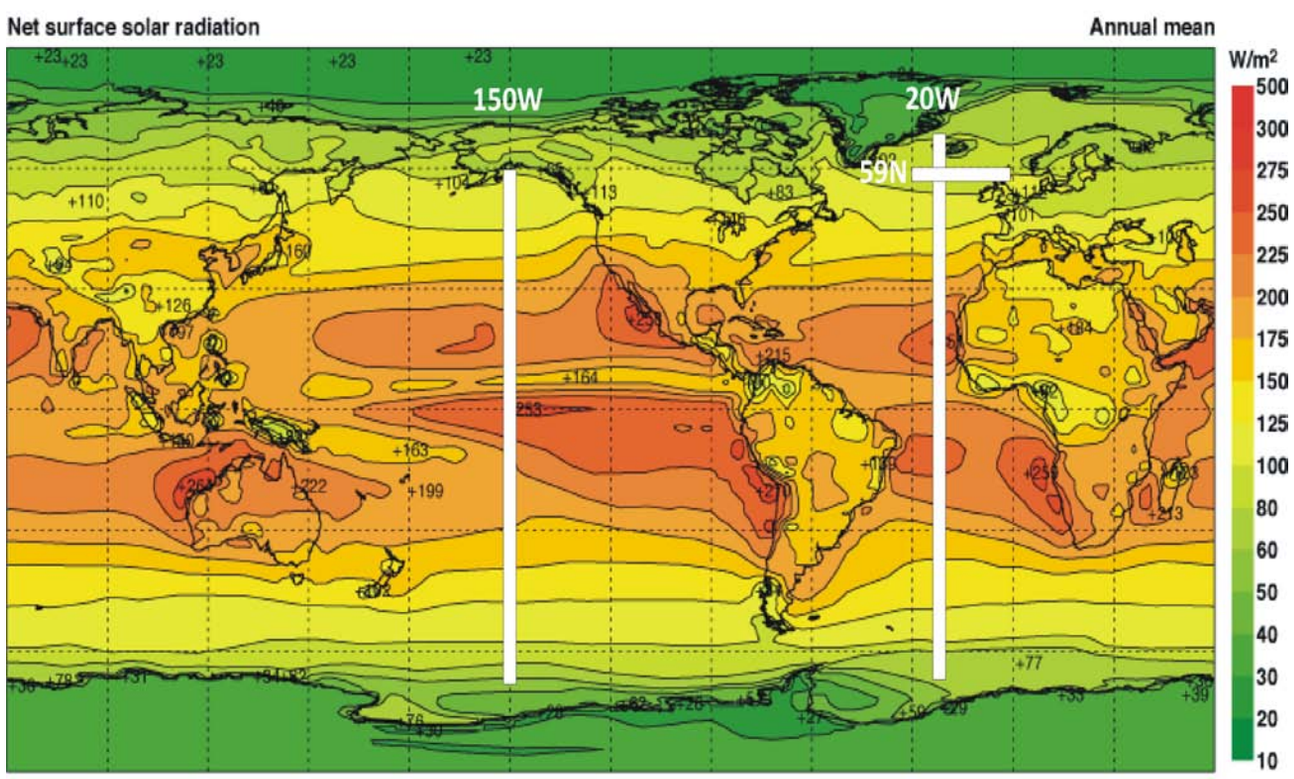

Figure 25: Annual mean net surface solar radiation (W/m^2), and the location of three profiles.

The Atlantic

Figure 26, for the Atlantic transect, reveals several interesting features, in particular a marked net cooling at the surface north of the Equator, and especially north of 25°N, where deeper layers (down to 1500 m depth) are also involved. At the Equator, and south of it, warming dominates at the surface, although cooling dominates at 50–250 m depth. The maximum Atlantic Ocean net warming over this period is found between 10 and 55°S, mainly affecting water depths between 200 and 1100 m. The warming in the South Atlantic is decreasing compared to the 2004–2018 diagram. Likewise, the net cooling north of 30°N is somewhat less pronounced in 2019 than in 2018.

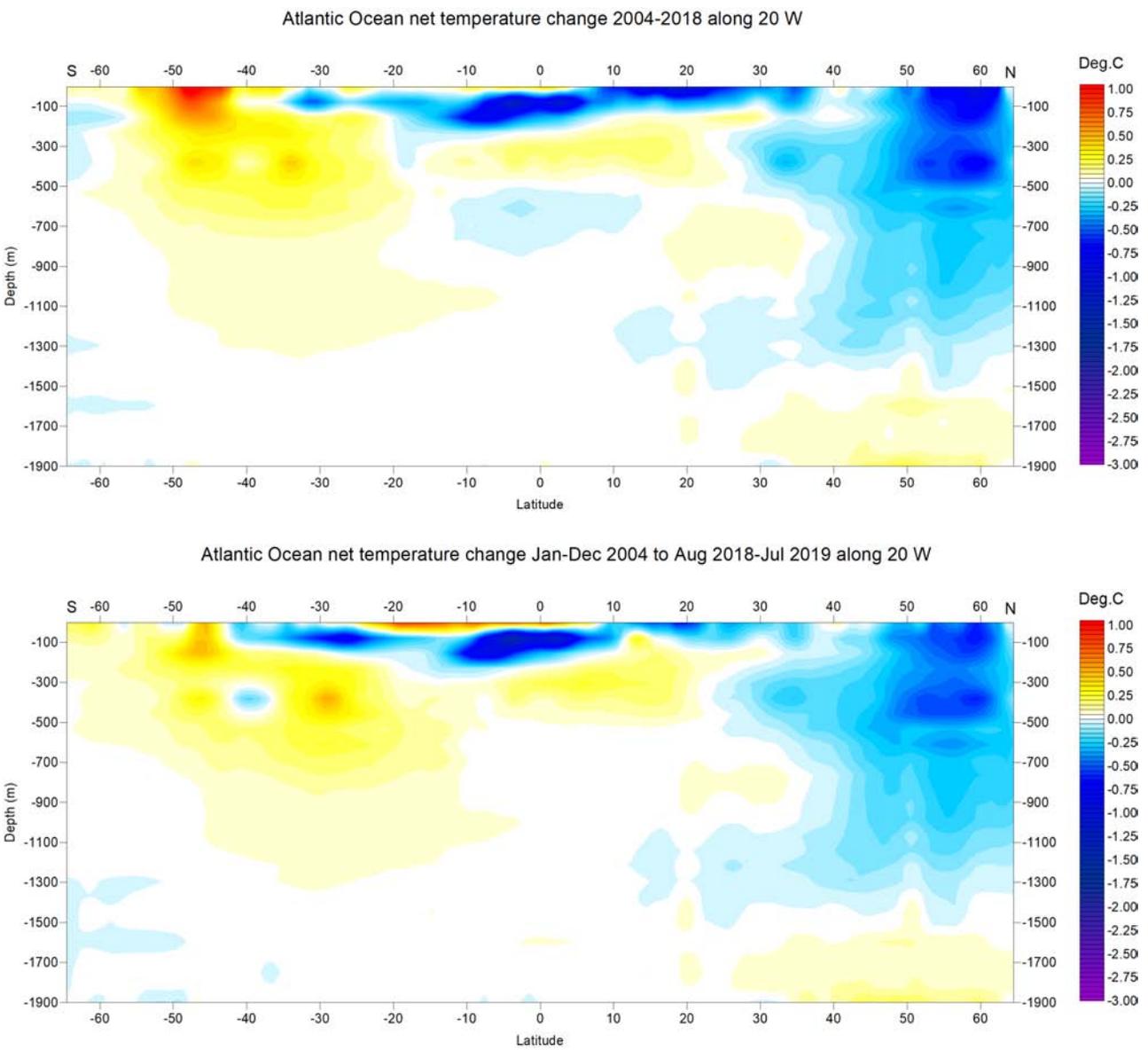

Figure 26: Net temperature change since 2004 from surface to 1900 m depth at 20°W in the Atlantic Ocean, using Argo data.

Top: 2004–2018, bottom: 2004–2019. See Figure 25 for geographical location of transect. Data source: Global Marine Argo Atlas.

The North Atlantic Current

Before moving on to the Pacific Ocean transect, it is also interesting to look at a short transect along the latitude 59°N, which crosses the North Atlantic Current, just south of the Faroe Islands (see Figure 25). This is important for weather and climate in much of Europe. Figure 27a shows a time series from 30°W to 0°W along that line, from the surface to 800 m depth. It thus represents a section across the water masses affected by the North Atlantic Current. Ocean temperatures higher than 9°C are shown by red colours.

This time series, although still relatively short, displays interesting dynamics. Warm water (above 9°C) apparently peaked in early 2006 and was followed by a gradual reduction until 2016. Since then, a partial temperature recovery has taken place. The observed change from peak to trough, playing out over approximately 11 years, might conceivably suggest the existence of an approximately 22-year temperature variation, but we will have to wait until the Argo series is somewhat longer before it will be possible to draw conclusions.

Figure 27b shows the same data (59°N, 30–0°W, 0–800 m depth, 2004–2018), plotted as a graph of depth-integrated average ocean temperature, in which the apparent cycle is clearer.

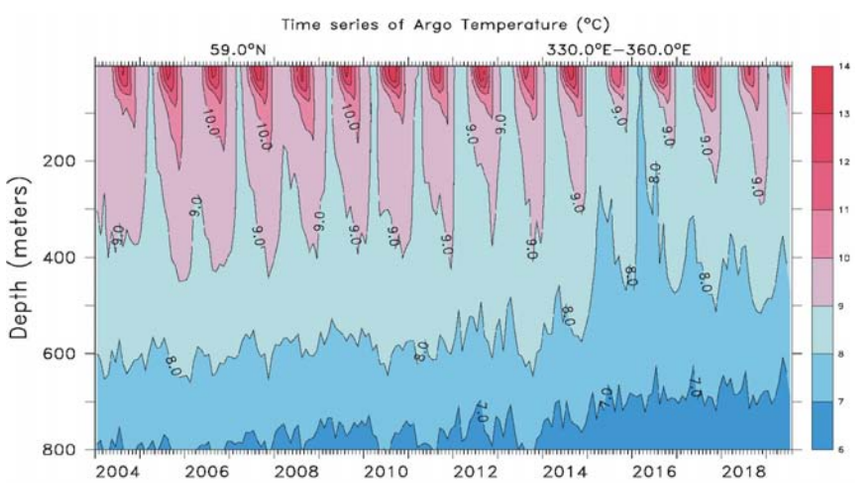

(a) Temperature profile by depth

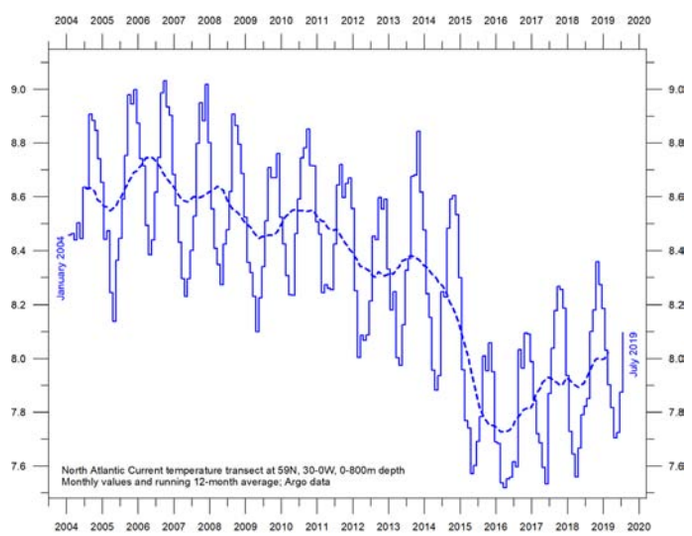

(b) Depth-integrated average ocean temperature

Figure 27: Temperature profile across the North Atlantic current.

Time series January 2004–July 2019 of ocean temperatures at 59°N, 30–0°W, from surface to 800 m depth, using Argo data. See Figure 25 for geographical location of transect. Source: Global Marine Argo Atlas.

The Pacific

Figure 28 shows the net changes 2004–2018/19 along 150°W, representing the Pacific, equivalent to Figure 26 for the Atlantic, prepared in the same way, and with the same caveats.

One prominent feature for 2019 is net cooling south of 35°S, affecting nearly all water depths down to 1900 m. However, compared to the 2004–2018 diagram, the cooling is becoming less pronounced and less widespread in the 2004–2019 diagram. Net cooling for 2004–2019 is especially pronounced in two bands, one north and one south of the Equator (at 25°S and 20°N), respectively, and both extending from the surface to 500 m. Net surface warming is taking place in three regions, centred on 50°S, the equator and 50°N, and especially affecting water depths down to about 500 m.

Neither the Atlantic or Pacific transects show to what extent any of the net changes are caused by ocean dynamics operating east and west of the two profiles considered. For that reason, the diagrams should not be overinterpreted. The two longitudinal transects suggest, however, an interesting contrast, with the Pacific Ocean mainly warming north of Equator, and cooling in the south, with the opposite happening in the Atlantic.

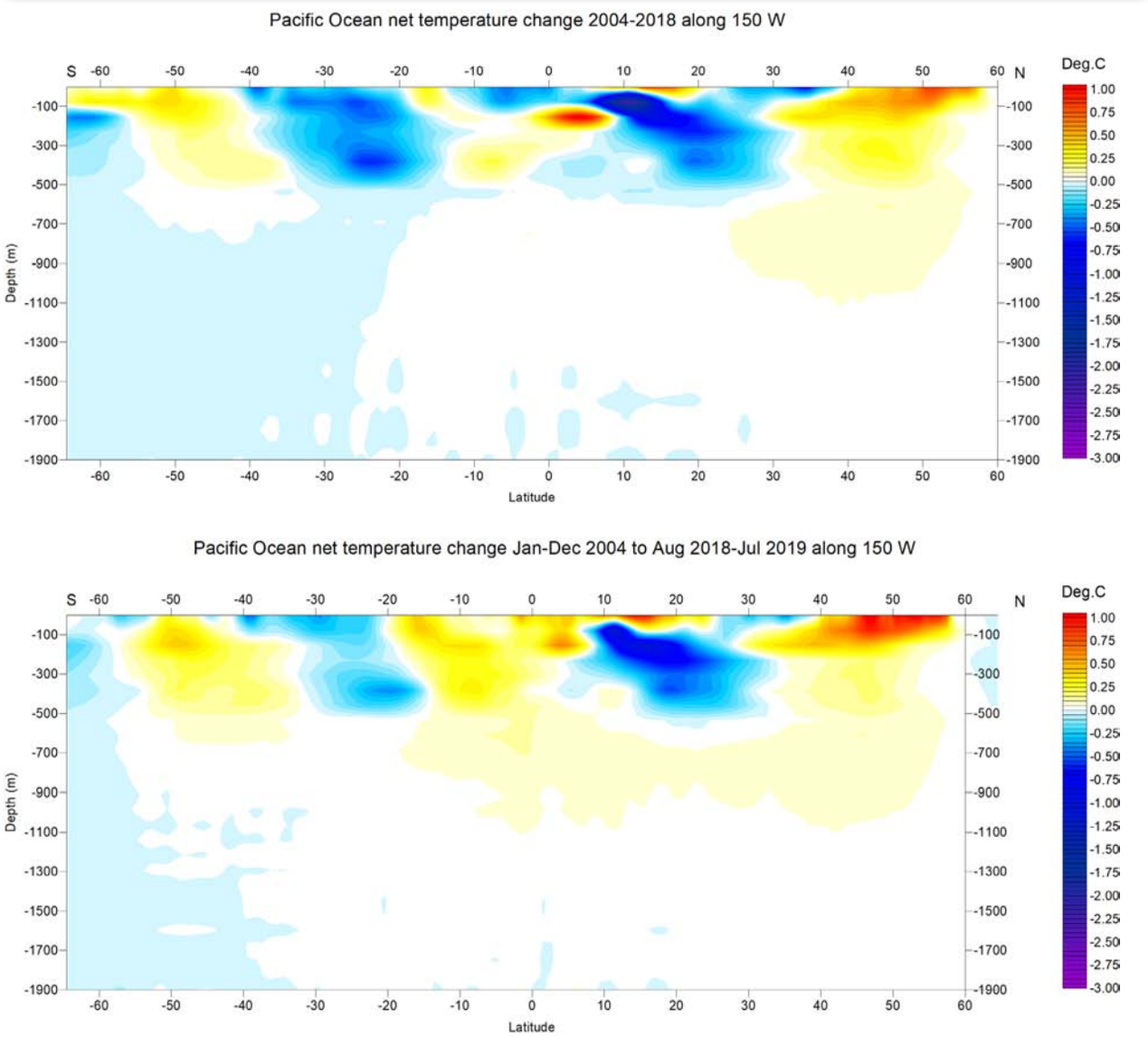

Figure 28: Net temperature change since 2004 from surface to 1900 m depth at 20°W in the Atlantic Ocean, using Argo data.

Top: 2004–2018, bottom: 2004–2019. See Figure 25 for geographical location of transect. Data source: Global Marine Argo Atlas.

4. Oceanic cycles

Southern Oscillation Index

Sustained negative values of the Southern Oscillation Index (SOI), as shown in Figure 29, often indicate El Niño episodes. Such negative values are usually accompanied by persistent warming of the central and eastern tropical Pacific Ocean, a decrease in the strength of the Pacific trade winds, and a reduction in rainfall over eastern and northern Australia.

Positive values of the SOI are usually associated with stronger Pacific trade winds and higher sea surface temperatures to the north of Australia, indicating La Niña episodes. Waters in the central and eastern tropical Pacific Ocean become cooler during this time. Eastern and northern Australia usually receive increased precipitation.

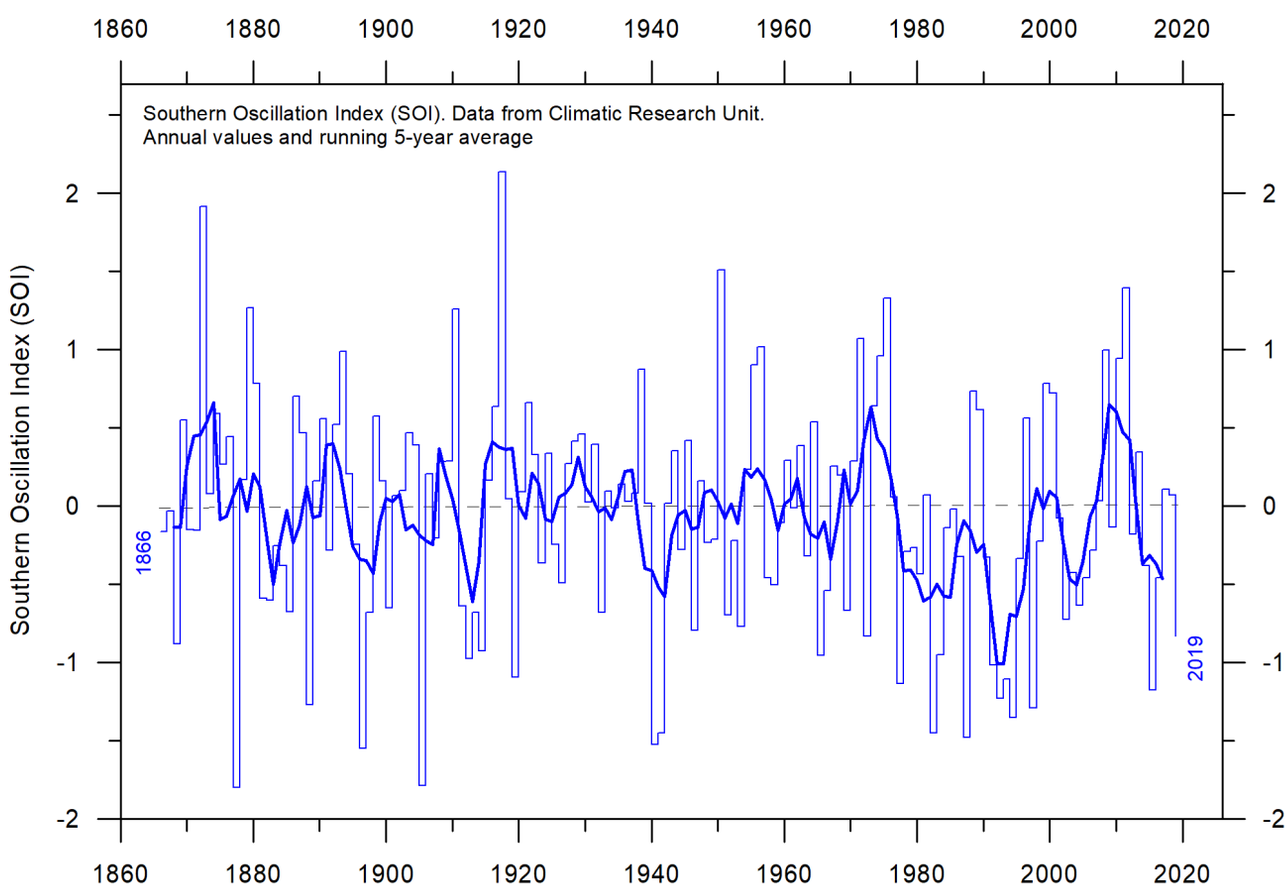

Figure 29: Annual Southern Oscillation Index (SOI) anomaly since 1866.

The Southern Oscillation Index (SOI) is calculated from the monthly or seasonal fluctuations in the air pressure difference between Tahiti and Darwin. The thin line represents annual values, while the thick line is the simple running 5-year average. Source: Climatic Research Unit, University of East Angila.

Pacific Decadal Oscillation

The Pacific Decadal Oscillation (PDO), shown in Figure 30, is a long-lived El Niño-like pattern of Pacific climate variability, with data extending back to January 1900. The causes of the PDO are not currently known, but even in the absence of a theoretical understanding, information about the oscillation improves season-to-season and year-to-year climate forecasts for North America because of its strong tendency for multi-season and multi-year persistence. The PDO also appears to be roughly in phase with global temperature changes. Thus, from a societal-impacts perspective, recognition of the PDO is important because it shows that 'normal' climate conditions can vary over time periods comparable to the length of a human lifetime.

The PDO nicely illustrates how global temperatures are tied to sea surface temperatures in the Pacific Ocean, the largest ocean on Earth. When sea surface temperatures are relatively low (the negative phase of the PDO), as they were from 1945 to 1977, global air temperature decreases. When sea surface temperatures are high (the positive phase of the PDO), as they were from 1977 to 1998, global surface air temperature increases (Figure 30).

A Fourier frequency analysis (not shown here) shows the PDO record to be influenced by a 5.7-year cycle, and possibly also by a longer cycle of about 53 years' duration.

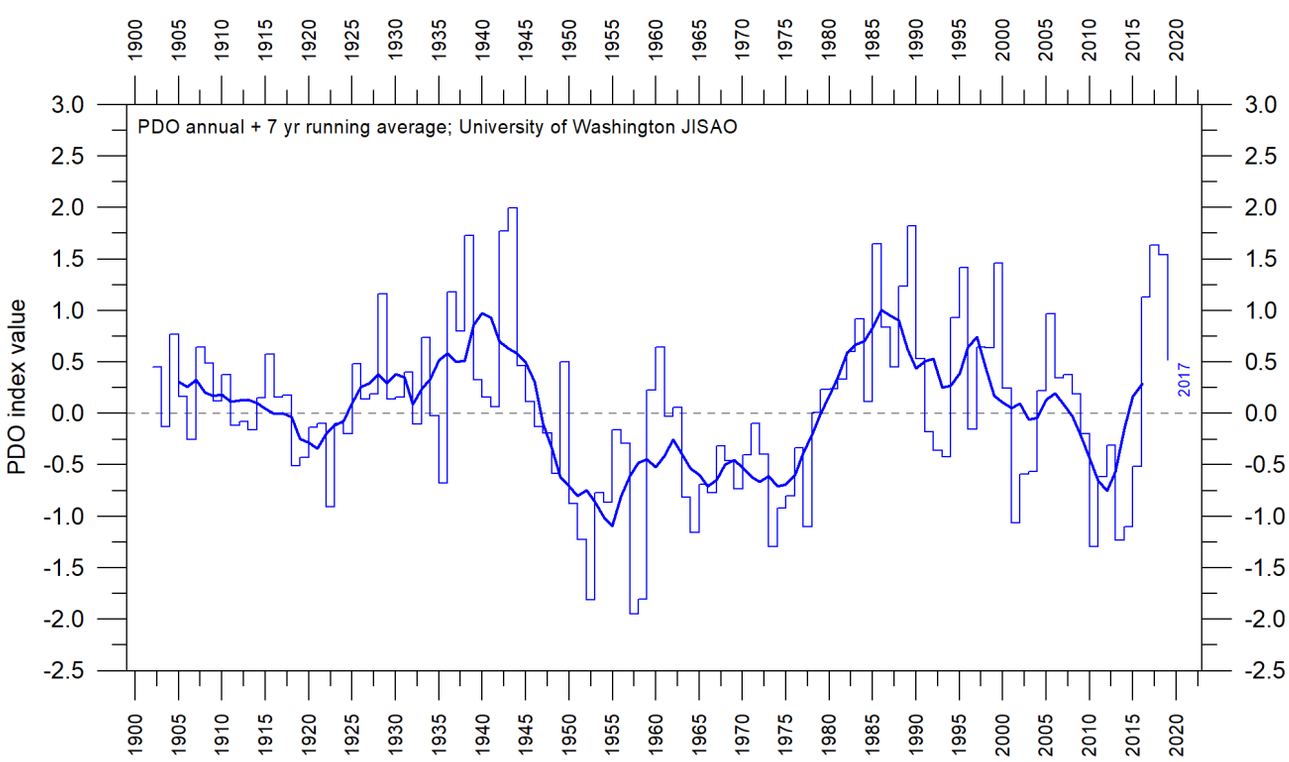

Figure 30: Annual values of the Pacific Decadal Oscillation (PDO).

The thin line shows the annual PDO values, and the thick line is the simple running 7-year average. Please note that the annual value of PDO is not yet updated beyond 2017. Source: Joint Institute for the Study of the Atmosphere and Ocean (JISAO), a cooperative Institute between the National Oceanic and Atmospheric Administration and the University of Washington, USA.

Atlantic Multidecadal Oscillation

The Atlantic Multidecadal Oscillation (AMO; Figure 31) is a mode of variability occurring in the North Atlantic Ocean sea surface temperature field. The AMO is basically an index of North Atlantic sea surface temperatures.

The AMO index appears to be correlated to air temperatures and rainfall over much of the Northern Hemisphere. The association appears to be high for north-eastern Brazil, rainfall in the African Sahel, and the summer climate in North America and Europe. The AMO index also appears to be associated with changes in the frequency of North American droughts and is reflected in the frequency of severe Atlantic hurricanes.

As one example, the AMO index may be related to the past occurrence of major droughts in the US Midwest and Southwest. When the AMO is high, these droughts tend to be more frequent or prolonged, and vice-versa for low values. Two of the most severe droughts of the 20th century in the US – the Dust Bowl of the 1930s and the 1950s droughts – occurred during periods of high AMO values. On the other hand, Florida and the Pacific Northwest tend to be the opposite; high AMO in these areas is associated with relatively high precipitation.

A Fourier-analysis (not shown here) shows the AMO record to be controlled by an 67-year cycle and, to a lesser degree, by a 3.5-year cycle.

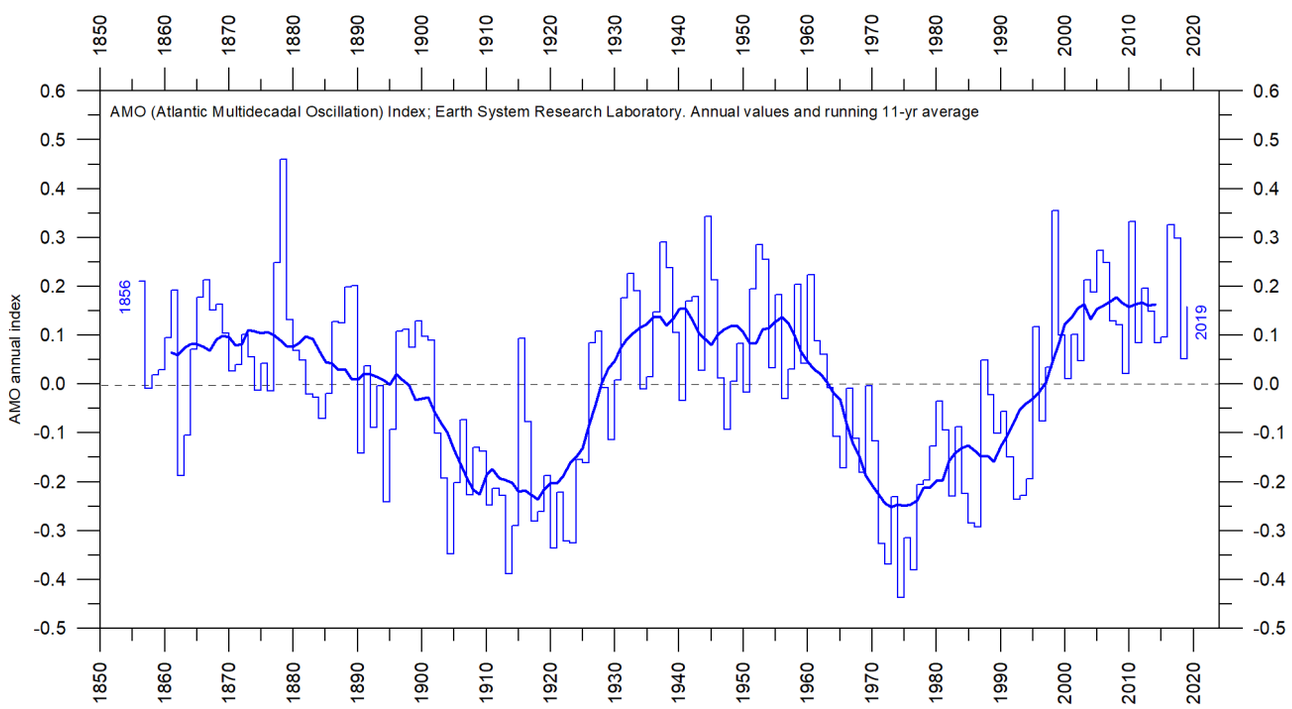

Figure 31: Annual Atlantic Multidecadal Oscillation.

Detrended and unsmoothed index values since 1856. The thin blue line shows annual values, and the thick line is the simple running 11-year average. Data source: Earth System Research Laboratory, NOAA, USA.

5. Sea level

Introduction

Global (or eustatic) sea-level change is measured relative to an idealised reference level, the geoid, which is a mathematical model of planet Earth's surface.[3] Global sea-level is a function of the volume of the ocean basins and the volume of water they contain. Changes in global sea-level are caused by – but not limited to – four main mechanisms:

- changes in local and regional air pressure and wind, and tidal changes introduced by the Moon;
- changes in ocean basin volume caused by tectonic (geological) forces;
- changes in ocean water density caused by variations in currents, water temperature and salinity;
- changes in the volume of sea water caused by changes in the mass balance of terrestrial glaciers.

In addition, there are subsidiary mechanisms influencing sea-level, such as storage of ground water, storage in lakes and rivers, evaporation, and so on.

Satellite altimetry measurements

Satellite altimetry is a relatively new and valuable type of measurement, with nearly global coverage. It provides unique insights into the detailed surface topography of the oceans and how it changes. However, it is probably not a precise tool for estimating absolute changes in global sea level due to assumptions that have to be made when interpreting the raw data. One of these (Figure 32) is the glacial isostatic adjustment (GIA). The GIA relates to large-scale, long-term mass transfer from the oceans to the land, in the form of rhythmic waxing and waning of the large Quaternary ice sheets in North America and North Europe. This enormous mass transfer causes rhythmic changes in surface load, resulting in viscoelastic mantle flow and elastic effects in the upper crust of the Earth. No single technique or observational network can give adequate information to allow a precise GIA to be estimated, so various assumptions have to be made. These assumptions are difficult to verify. They depend on the deglaciation model used (for the last glaciation) and upon the model of the crust-mantle used. Because of this (and additional factors), interpretations of modern global sea-level change based on satellite altimetry vary from about 1.9 mm/year to about 3.5 mm/year.

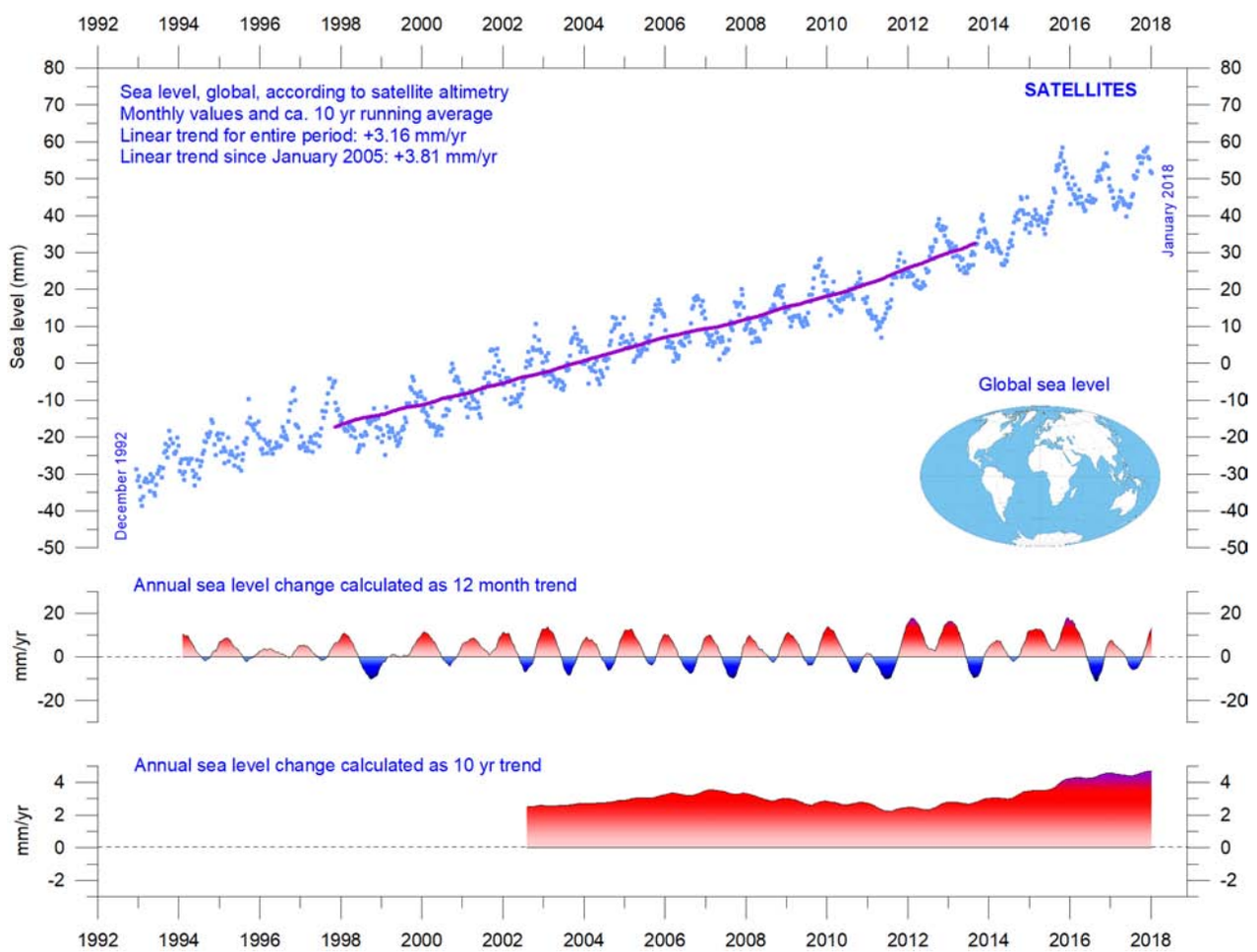

Figure 32: Global sea-level change since December 1992.

The blue dots are the individual observations, and the purple line represents the running 121-month (ca. 10-year) average. The two lower panels show the annual sea level change, calculated for 1- and 10-year time windows, respectively. These values are plotted at the end of the interval considered. Source: Colorado Center for Astrodynamics Research at University of Colorado at Boulder.

Tide-gauge measurements

Tide gauges, located at coastal sites, record the net movement of the local ocean surface in relation to the land. Measurements of local relative sea-level change (Figure 33) are vital for coastal planning, and it is tide-gauge data, rather than satellite altimetry, that are relevant for planning purposes in coastal areas.

In a scientific context, the net movement of the local sea-level, as measured by the tide gauges, comprises two components:

- the vertical change of the ocean surface
- the vertical change of the land surface.

For example, a tide gauge may record an apparent sea-level increase of 3 mm/year. If geodetic measurements show the land to be sinking by 2 mm/year, the real sea level rise is only 1 mm/year (3 minus 2 mm/year). In a global sea-level change context, the value of 1 mm/year is relevant, but in a local coastal planning context the 3 mm/year value obtained from the tide gauge is the only relevant factor.

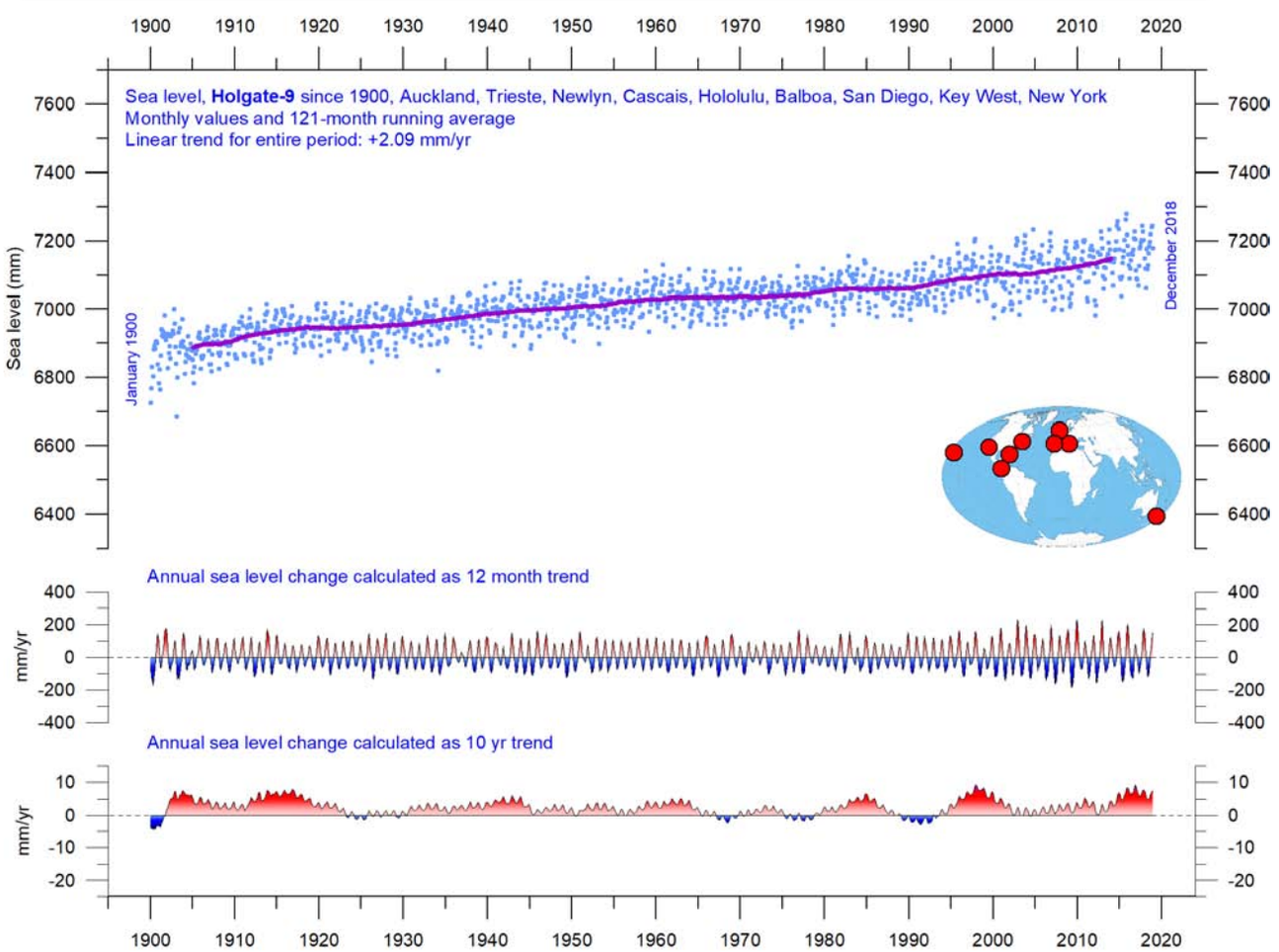

Figure 33: Holgate-9 monthly tide gauge data.

Source: PSMSL Data Explorer. Holgate (2007) suggested the nine stations listed in the diagram captured the variability found in a larger number of stations over the last half century. For that reason, average values of the Holgate-9 group of tide gauge stations are interesting to follow, even though Auckland (New Zealand) has not reported data since 2000, and Cascais (Portugal) since 1993. Unfortunately, because of this data loss, the Southern Hemisphere is underweighted in the Holgate-9 series since 2000. The blue dots represent individual average monthly observations, and the purple line represents the running 121-month (ca. 10-year) average. The two lower panels show the annual sea level change, calculated for 1- and 10-year time windows, respectively. These values are plotted at the end of the interval considered.

To construct a time series of sea-level measurements at each tide gauge, the monthly and annual means must be reduced to a common datum. This reduction is performed by the Permanent Service for Mean Sea Level, using the tide gauge datum history provided by the supplying national authority. The Revised Local Reference datum at each station is defined to be approximately 7000 mm below mean sea level, with this arbitrary choice made many years ago to avoid negative numbers in the resulting monthly and annual mean values.

Few places on Earth are completely stable, and most tide gauges are located at sites exposed to tectonic uplift or sinking (the vertical change of the land surface). This widespread vertical instability has several causes, but of course affects the interpretation of data from individual tide gauges. Much effort is put into correcting for local tectonic movements.

Data from tide gauges located at tectonically stable sites is therefore of particular interest for determining real short- and long-term sea-level change. One long record from such a site comes from Korsør, Denmark (Figure 34). This record indicates a stable sea-level rise of about 0.83 mm per year since January 1897, without any indication of recent acceleration.

Data from tide gauges all over the world suggest an average global sea-level rise of 1.0–1.5 mm/year, while the satellite-derived record (Figure 32) suggests a rise of about 3.2 mm/year, or more. The noticeable difference (at least 1:2) between the two datasets is remarkable but has no broadly accepted explanation. It is, however, known that satellite observations are subject to several complications in areas near the coast.[4]

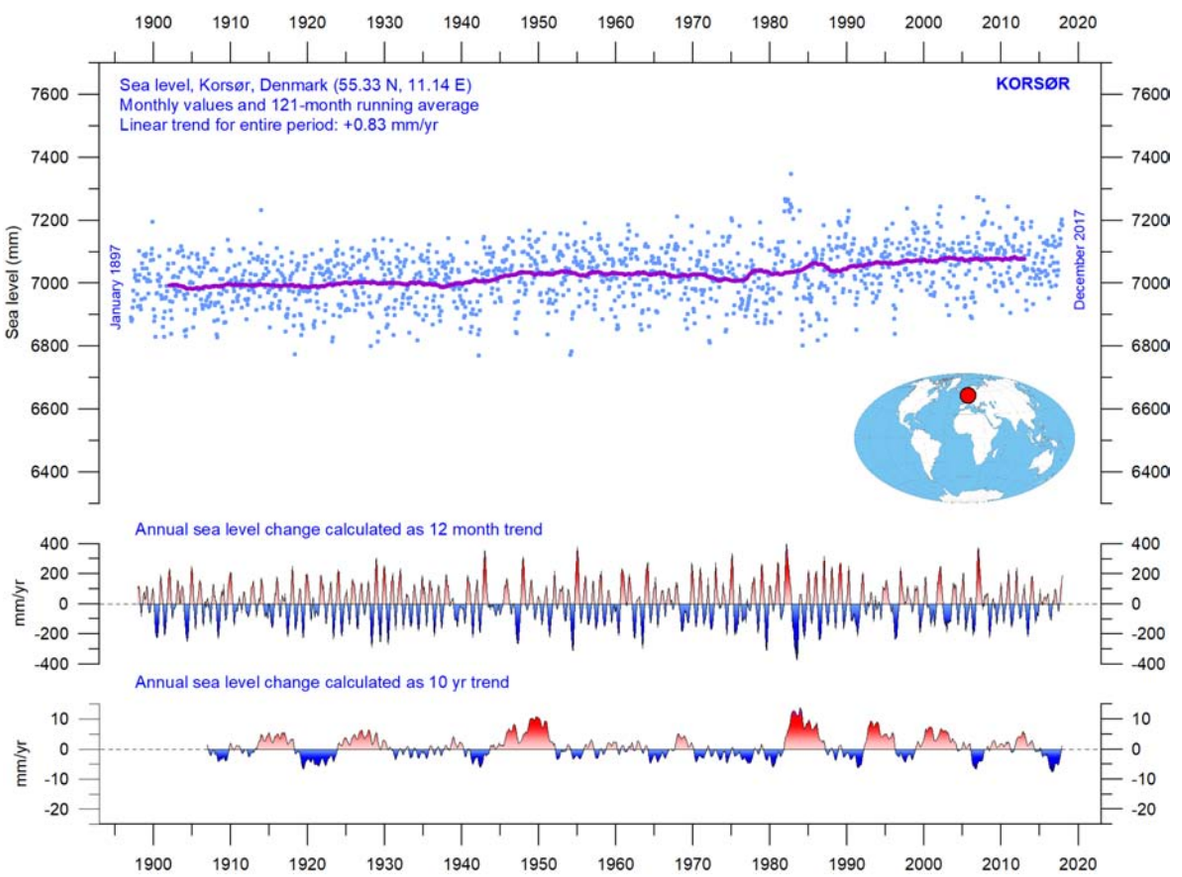

Figure 34: Korsør (Denmark) monthly tide gauge data.

Source: PSMSL Data Explorer. The blue dots are the individual monthly observations, and the purple line represents the running 121-month (ca. 10-year) average. The two lower panels show the annual sea-level change, calculated for 1- and 10-year time windows, respectively. These values are plotted at the end of the interval considered.

6. Sea-ice extent

Figure 35 shows average sea-ice extent graphs for the two poles in the period 1979–2019. There are contrasting trends in the Arctic and Antarctic. The Northern Hemisphere has tended towards lower sea-ice extent, but there was a simultaneous increase in the Southern Hemisphere, at least until 2016, after which there was an extraordinarily rapid decrease during the Southern Hemisphere spring of 2016. The reduction was much faster than in any previous spring season during the satellite era, and was seen in all sectors of the

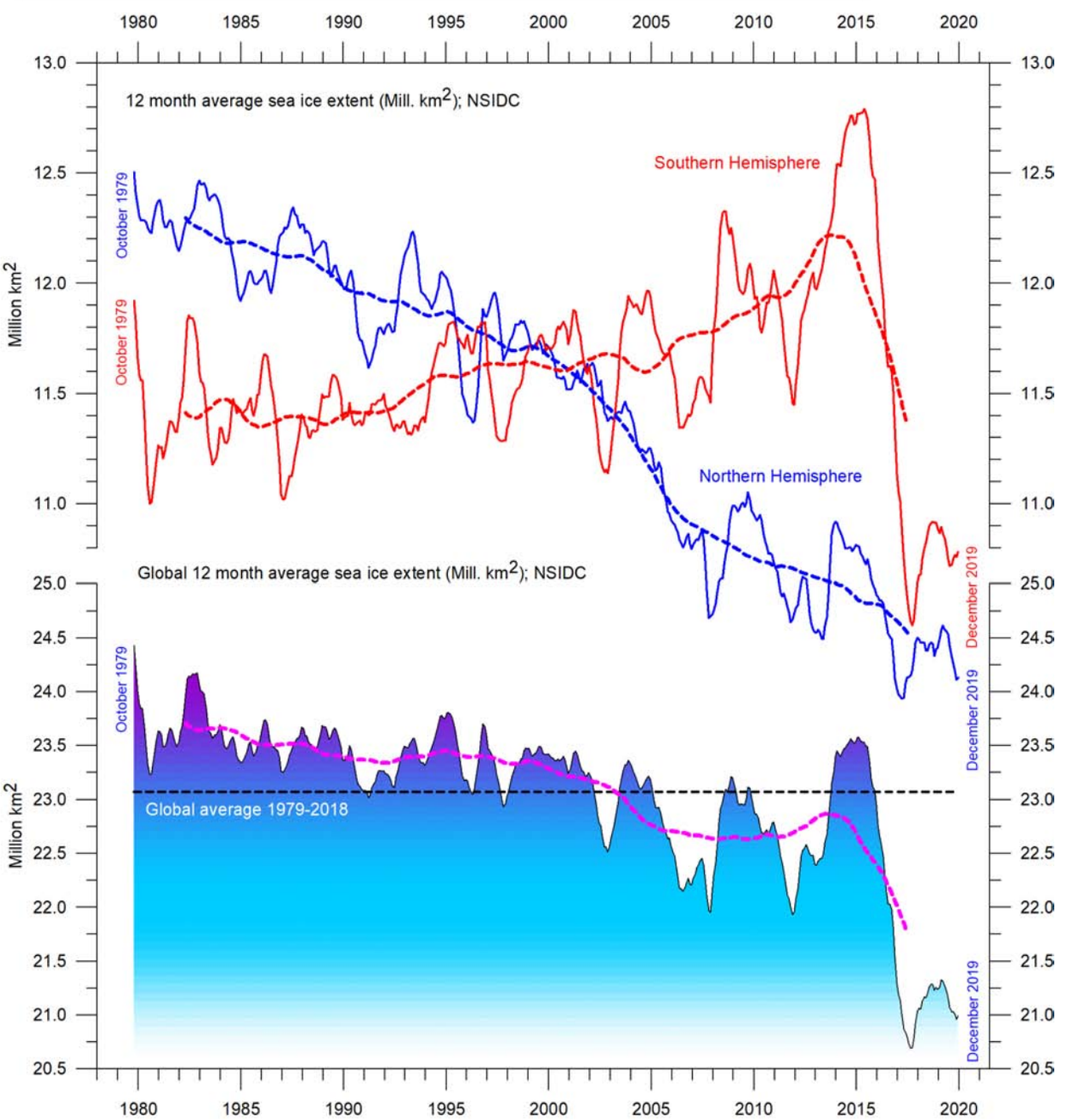

Figure 35: Global and hemispheric 12-month running average sea-ice extent since 1979.

The October 1979 value represents the monthly average of November 1978–October 1979, the November 1979 value represents the average of December 1978–November 1979, etc. The stippled lines represent a 61-month (ca. 5-year) average. The last month included in the 12-month calculations is shown to the right in the diagram. Data source: National Snow and Ice Data Center (NSIDC).

Antarctic, but particularly in the Weddell and Ross Seas. In these sectors, strong northerly (warm) surface winds pushed the sea ice back towards the Antarctic continent. The unusual wind conditions in 2016 have been discussed in the literature,[5] and appear to be related to natural climate variability. The satellite sea-ice record is still short, and does not fully represent natural variations playing out over more than a decade or two.

What can be identified from record is nevertheless instructive. Both 12-month average graphs (Figure 35) exhibit recurring variations that are superimposed on the overall trends. The Arctic sea ice is strongly influenced by a 5.3-year periodic variation, and the Antarctic sea ice by a periodic variation of about 4.5 years. Both of these variations reached their minima simultaneously in 2016, which at least partly explains the simultaneous minimum in global sea-ice extent.

In the coming years these cycles may induce an increase in sea-ice extent at both poles, with a consequent increase in the global total. In fact, this trend may already have started (Figure 35). However, in coming years, the minima and maxima for these variations will not occur synchronously because of their different periods, and the global minimum (or maximum) may therefore be less pronounced than in 2016.

Figure 36 shows the overall extent and thickness of the Arctic sea ice from the end of 2018 to the end of 2019, as published by the Danish Meteorological Institute. The most conspicuous change has been an overall increase in sea ice in parts of the Europe–Russia sector of the Arctic Ocean. In addition, relatively thick sea ice moved into the Svalbard-Franz Josef Islands sector in 2019, compared to the situation at the end of 2018. North of Canada and Greenland, however, thick ice has partly drifted away.

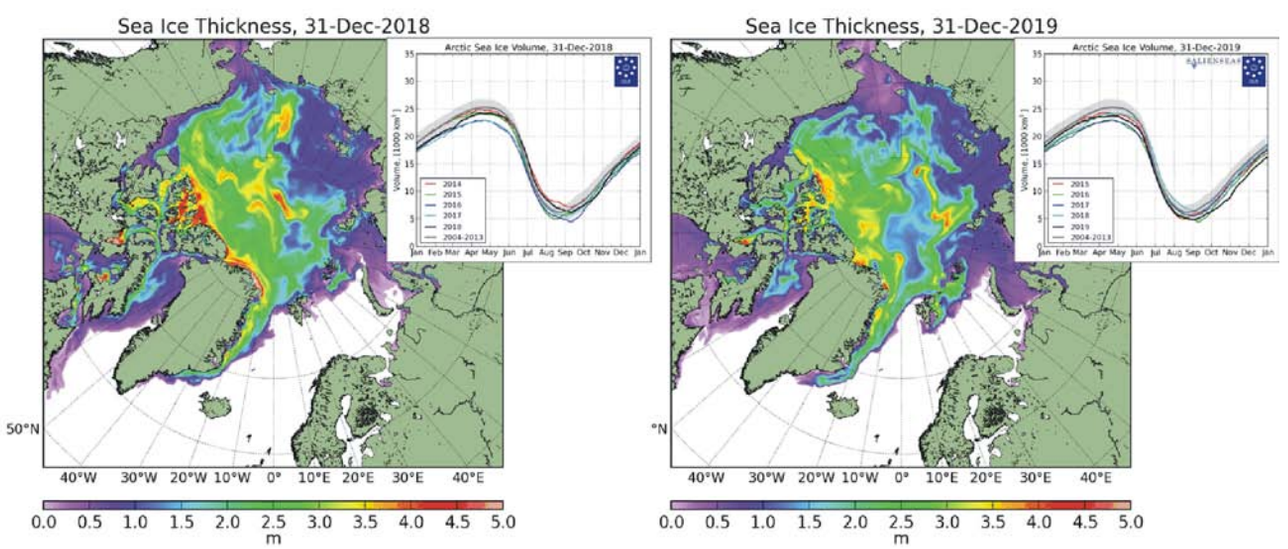

Figure 36: Arctic sea-ice extent and thickness.

31 December 2018 (left) and 2019 (right) and the seasonal cycles of the calculated total arctic sea-ice volume, according to the Danish Meteorological Institute (DMI). The mean sea-ice volume and standard deviation for the period 2004–2013 are shown by grey shading in the insert diagrams.

7. Snow cover

Variations in global snow cover are mainly a function of changes in the Northern Hemisphere (Figure 37), where all the major land areas are located. The Southern Hemisphere snow cover extent is essentially controlled by the Antarctic Ice Sheet, and therefore relatively stable.

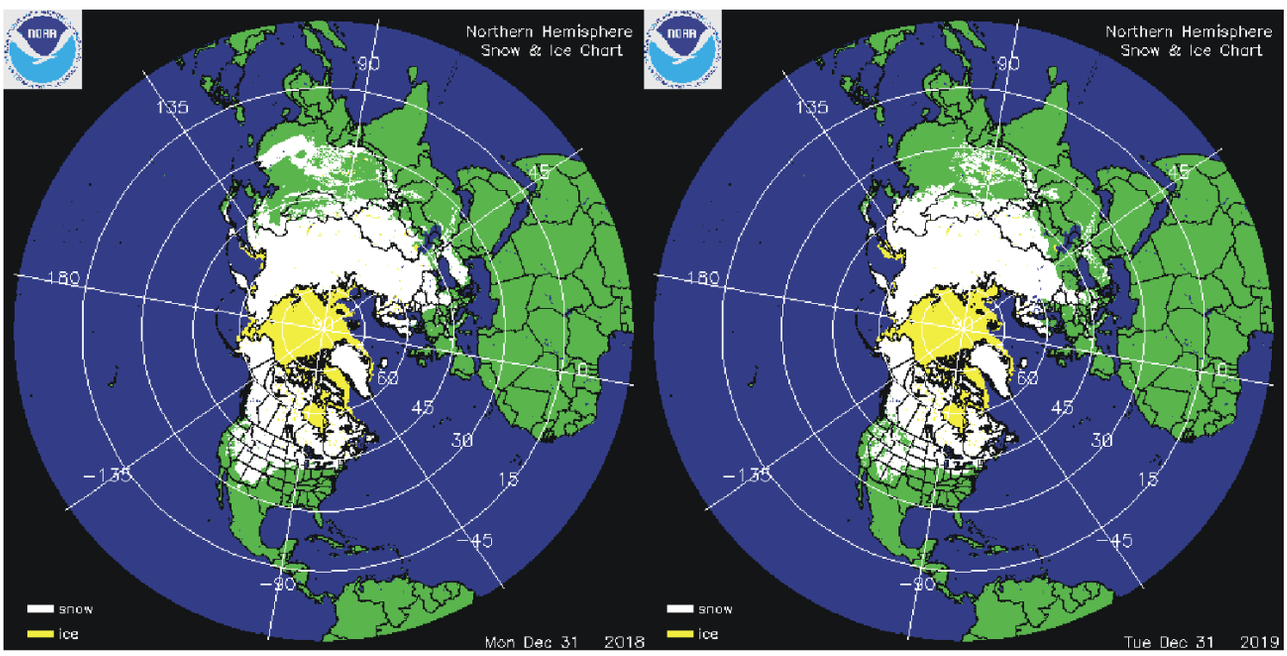

31 December 2018 31 December 2019

Figure 37: Arctic sea-ice extent and thickness.

Source: National Ice Center (NIC).

The Northern Hemisphere snow-cover extent is subject to large local and regional variations from year to year. However, the overall tendency since 1972 is stability, as illustrated in Figures 38 and 39.

During the Northern Hemisphere summer, the snow cover usually shrinks to about 2,400,000 km^2 (principally controlled by the size of the Greenland Ice Sheet), and during the Northern Hemisphere winter it increases to about 50,000,000 km^2, representing no less than 33% of planet Earth's total land area (Figure 38).

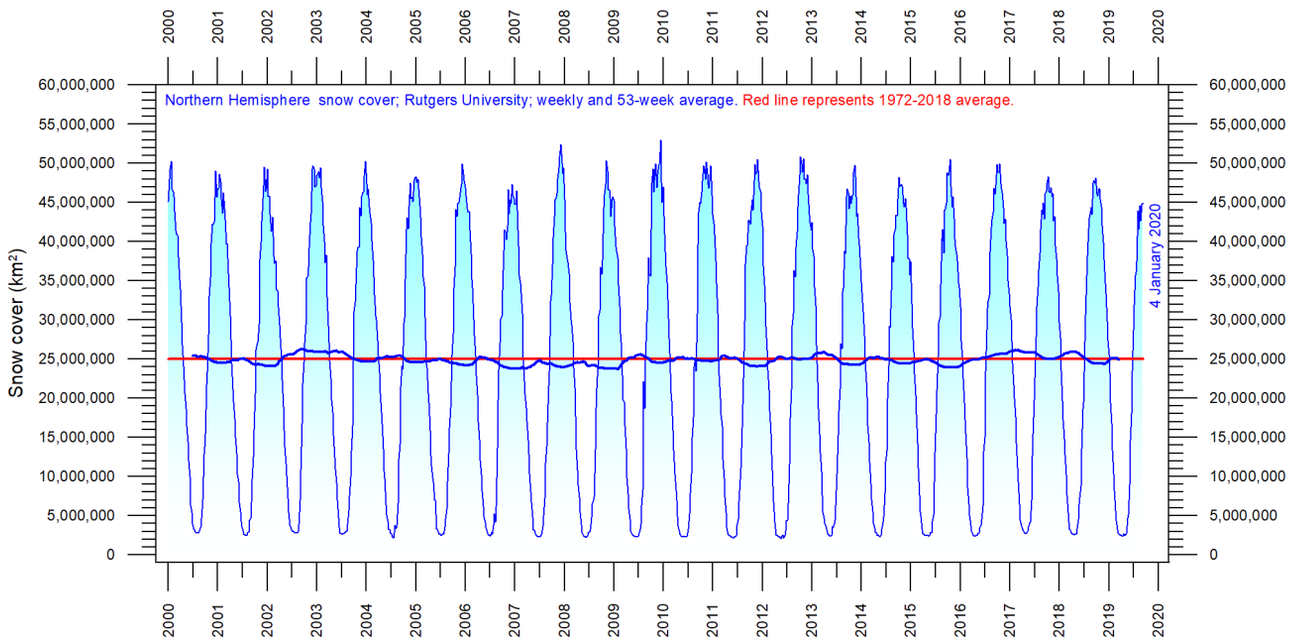

Since January 2000

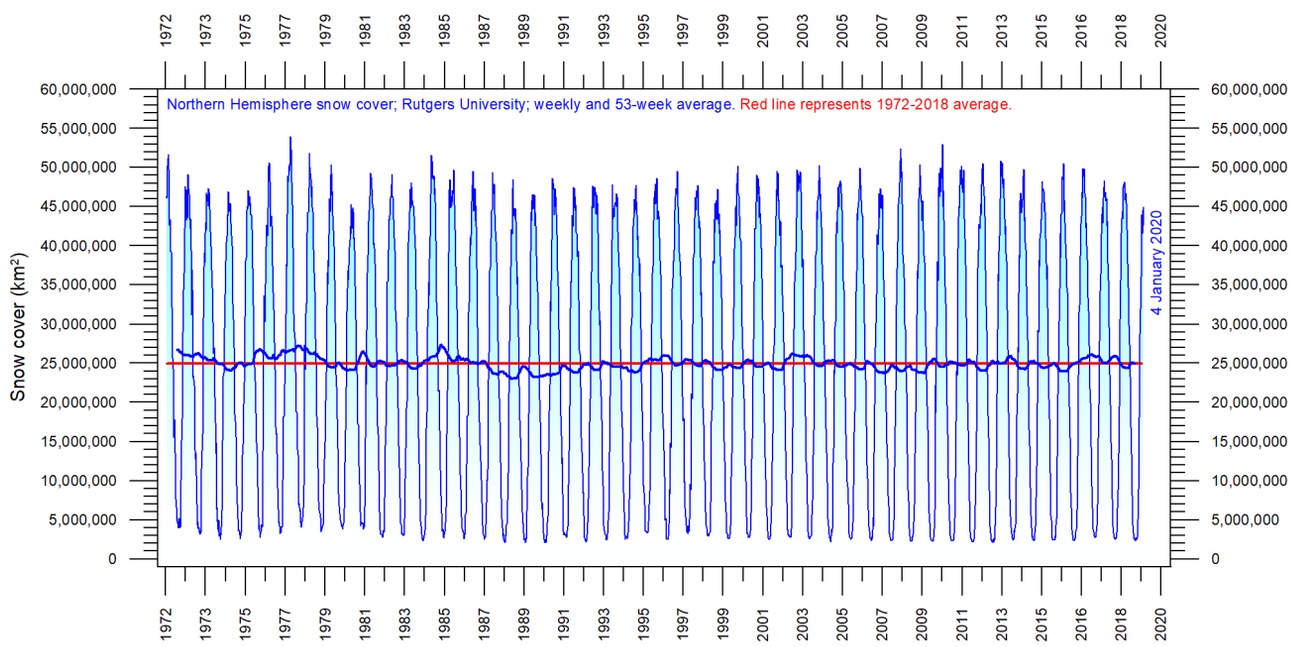

Since January 1972

Figure 38: Northern Hemisphere weekly snow cover extent.

Source: Rutgers University Global Snow Laboratory. The thin blue line is the weekly data, and the thick blue line is the running 53-week average (approximately 1 year). The horizontal red line is the 1972–2018 average.

Figure 39 shows trends in seasonal snow cover in the Northern Hemisphere. Autumn extent is increasing slightly, mid-winter extent is basically stable, and spring extent is decreasing slightly. In 2019, Northern Hemisphere snow-cover extent was similar to 2018.

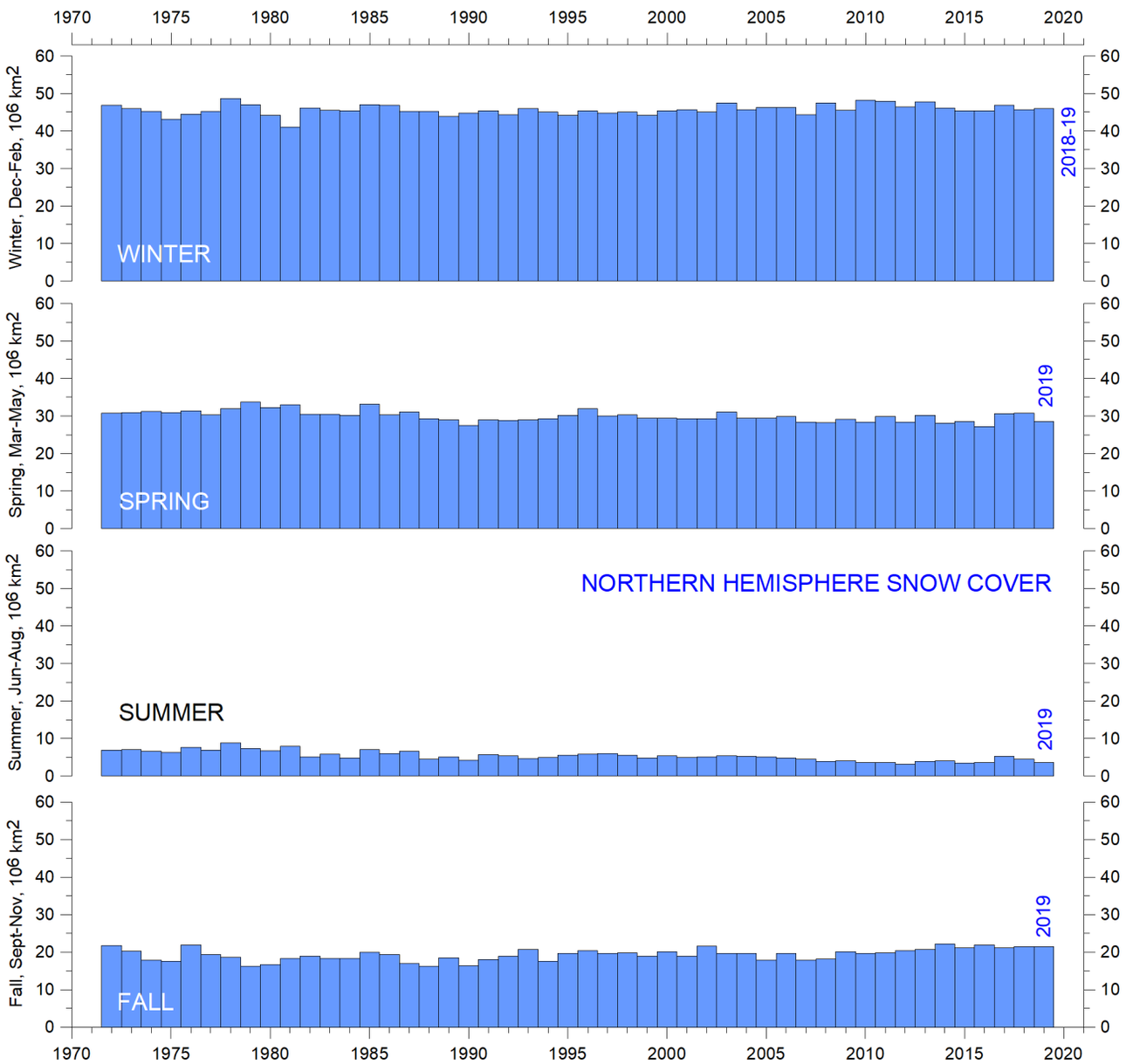

Figure 39: Northern Hemisphere weekly snow cover extent.

Source: Rutgers University Global Snow Laboratory.

8. Storms

Tropical storms and hurricanes

Accumulated cyclone energy (ACE) is a measure used by the US National Oceanic and Atmospheric Administration to express the activity of individual tropical cyclones and entire tropical cyclone seasons. ACE is calculated as the square of the wind speed every 6 hours and is then scaled by a factor of 10,000 for usability, using a unit of 10^4 knots^2. The ACE of a season is the sum of the ACE for each storm and thus encapsulates the number, strength, and duration of all the tropical storms in the season.

The damage potential of a hurricane is proportional to the square or cube of the maximum wind speed, and thus ACE is therefore not only a measure of tropical cyclone activity, but also a measure of the damage potential of an individual cyclone or a season. Existing records (Figure 40) do not suggest any abnormal cyclone activity in recent years.

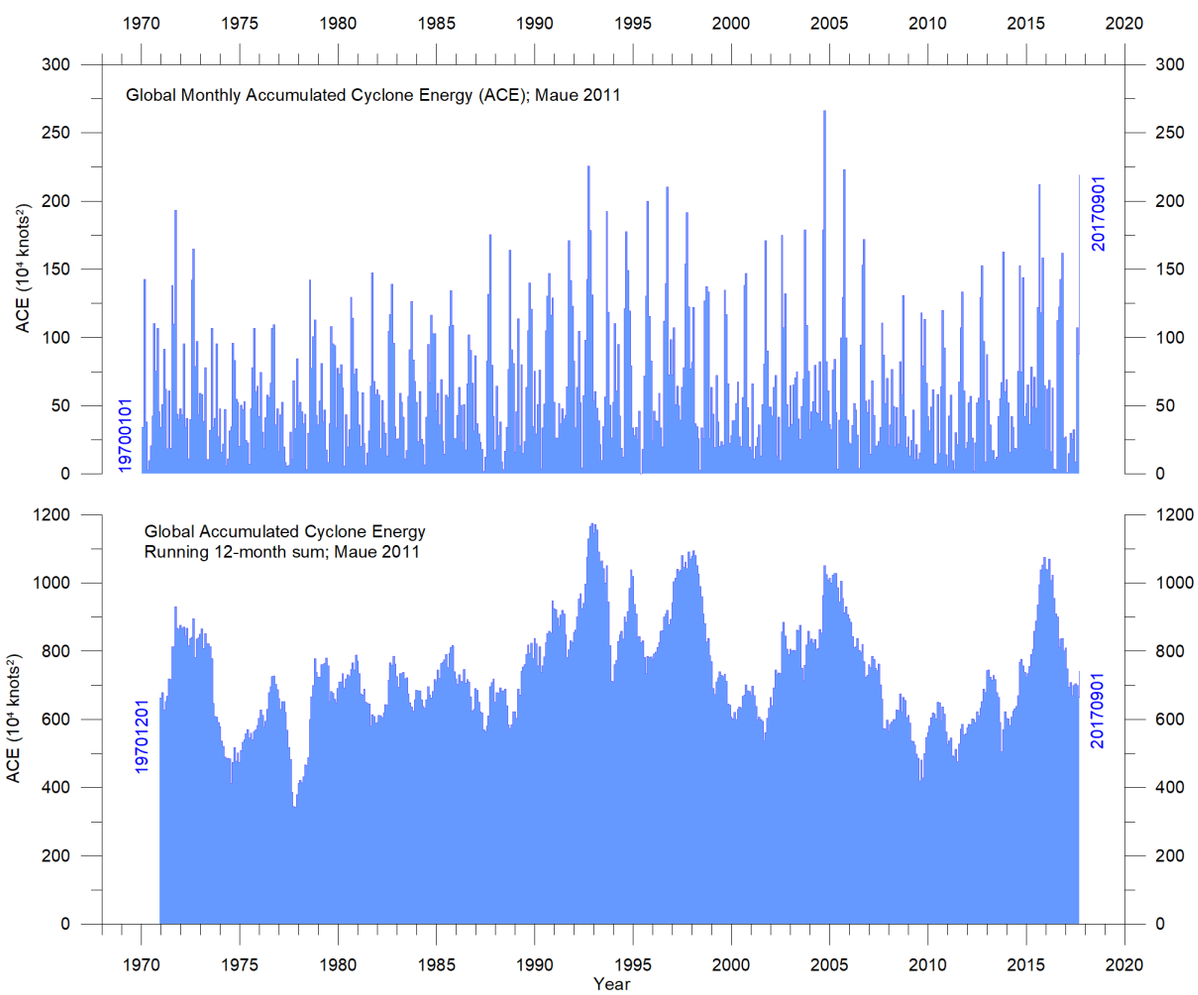

Figure 40: Global hurricane ACE since January 1970.

Top: monthly and bottom: running 12-month sums. The running 12-month sum (lower panel) is plotted at the end of the time interval considered. Data source: Updated from Maue (2011) ACE data. Please note that these data are not yet updated beyond September 2017.

The global ACE data display a variable pattern over time (Figure 40), but again without any clear trend. This is also true of the equivalent records for the Northern and Southern Hemispheres (Figures 41 and 42). The period 1992–1998 was characterised by high values; other peaks were seen in 2004–2005, and in 2016, while the periods 1973–1990 and 2012–2015 were characterised by low values. The peaks in 1998 and 2016 coincided with strong El Niño events in the Pacific Ocean (see Section 3).[6]

The Northern Hemisphere ACE (Figure 41) dominates the global signal (Figure 40) and therefore exhibits similar peaks and troughs as the global data, without any clear trend for the entire observational period. The Northern Hemisphere's main cyclone season is June–November.

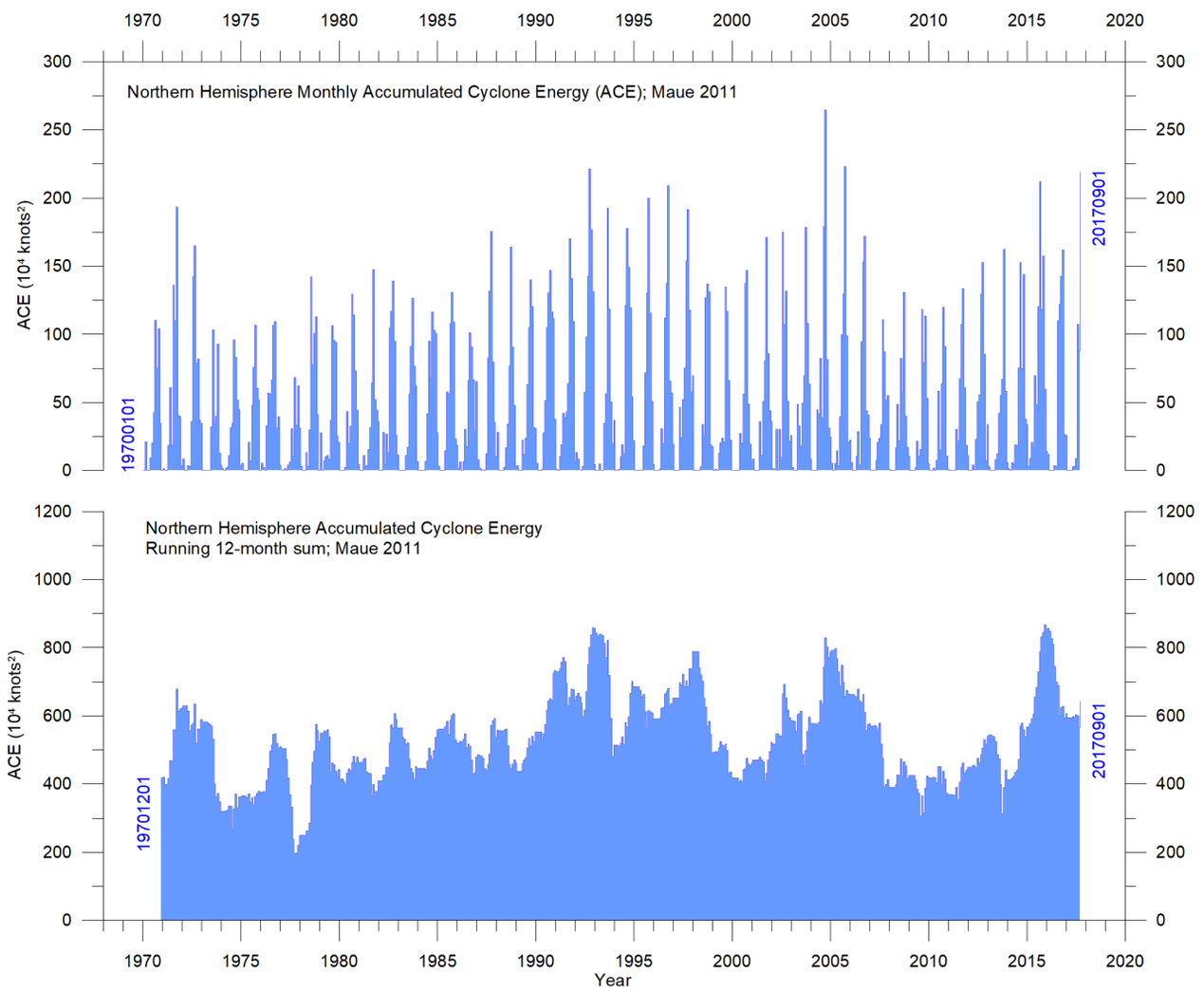

Figure 41: Northern Hemisphere hurricane ACE since January 1970.

Top: monthly and bottom: running 12-month sums. The running 12-month sum (lower panel) is plotted at the end of the time interval considered. Source: Updated from Maue (2011) ACE data. Please note that these data are not yet updated beyond September 2017.

The Southern Hemisphere ACE values (Figure 42) are lower than for the Northern Hemisphere, and the main cyclone season is December–April.

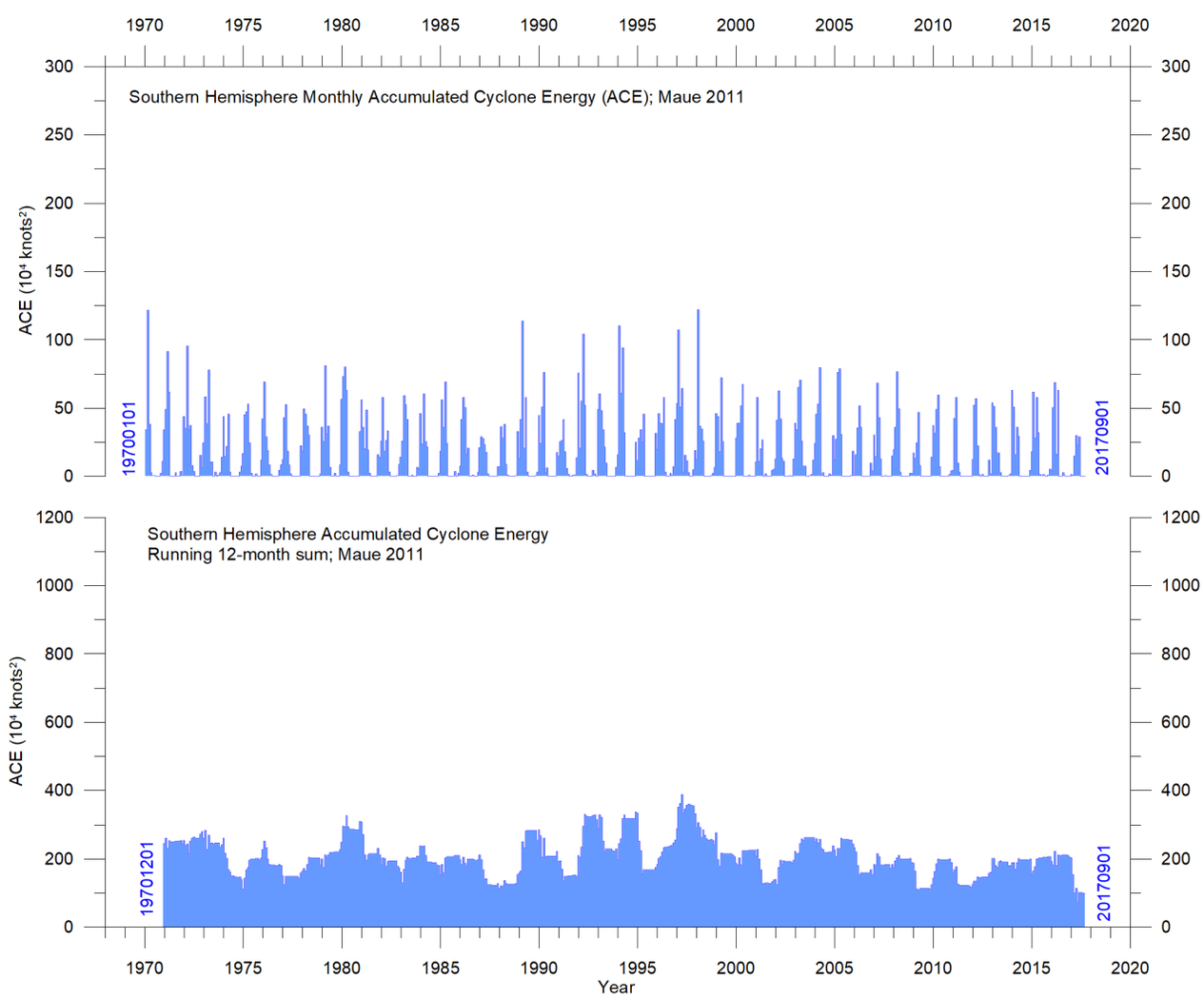

Figure 42: Southern Hemisphere hurricane ACE since January 1970.

Top: monthly and bottom: running 12-month sums. The running 12-month sum (lower panel) is plotted at the end of the time interval considered. Data source: Updated from Maue (2011) ACE data. Please note that these data are not yet updated beyond September 2017.

The Atlantic Oceanographic and Meteorological Laboratory ACE data series goes back to 1850. A Fourier analysis (not shown) for the Atlantic Basin (Figure 43) suggests that the ACE series is strongly influenced by a periodic variation of about 60 years' duration. Since 2002, the Atlantic ACE series has had a declining trend, but with large interannual variations. The North Atlantic hurricane season often exhibits above-average activity in La Niña conditions during late summer (August–October), as was the case in 2017.[7]

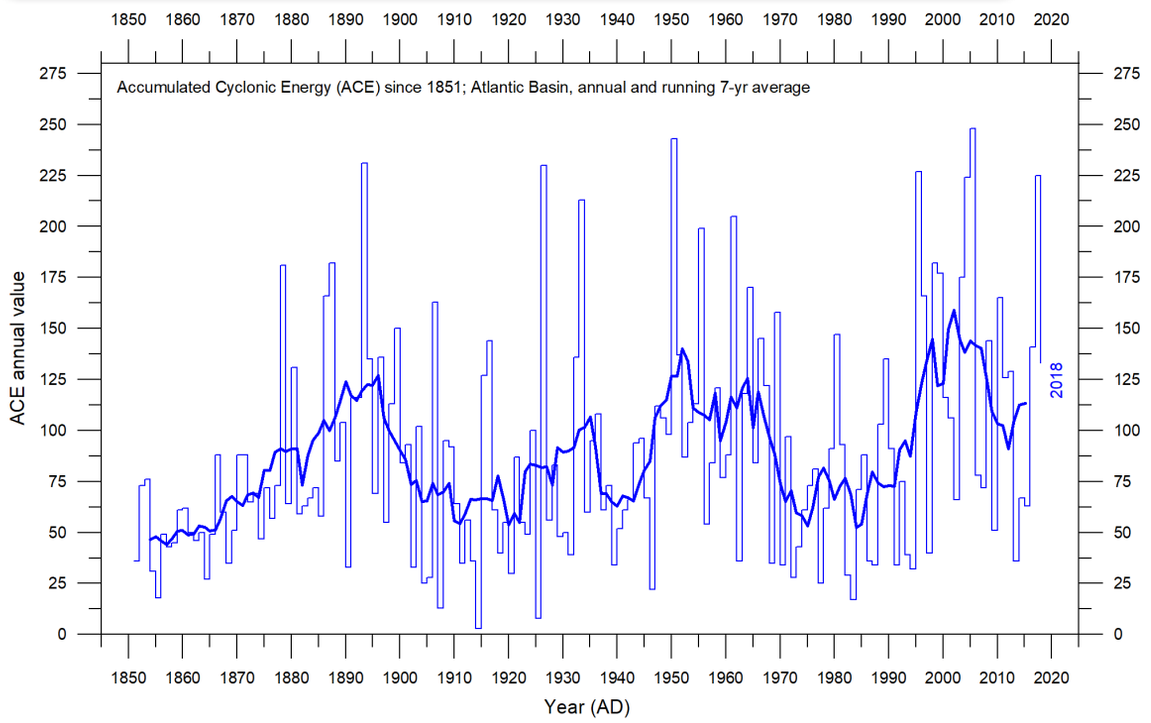

Figure 43: ACE for Atlantic basin per year since 1850 AD.

Thin lines show annual ACE values, and the thick line shows the running 7-year average. Data source: Atlantic Oceanographic and Meteorological Laboratory, Hurricane Research Division, NOAA. Please note that these data are not yet updated beyond 2018.

Other storms and wind

The number of hurricane landfalls in the continental USA is shown in Figure 44. Over the observational period, this data series shows considerable variations from year to year, but it is not possible to detect any clear trend. A Fourier analysis (not shown) reveals two statistically significant cycles, of about 3.2 and 4.9 years' duration.

An insight into changes in prevailing wind conditions may also be obtained from the inspection of observations carried out at coastal meteorological stations. One example of such a record comes from the Lista Lighthouse. The lighthouse sits on an exposed cape at the extreme southwestern edge of the mainland of Norway, and is representative of wind conditions in the North Sea and the European sector of the North Atlantic. Lista Lighthouse has a monthly wind record going back to January 1931 (Figure 45). At this location, the strongest winds were recorded shortly

after World War II, since when they have declined somewhat. This, to some degree, reflects a similar trend in the number of landfalling hurricanes in the continental USA (Figure 45), on the opposite shore of the North Atlantic.

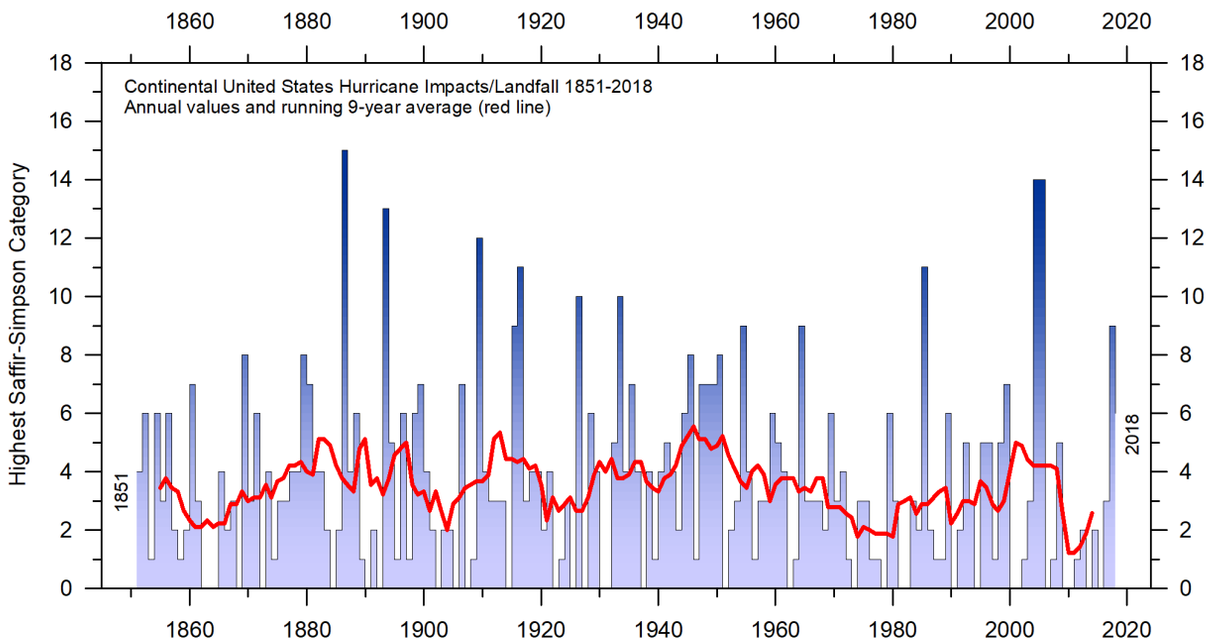

Figure 44: Number of continental United States hurricane impacts/landfalls 1851–2018.

The highest Saffir-Simpson Hurricane Scale impact in the United States is based upon estimated maximum sustained surface winds produced at the coast. Data source: Hurricane Research Division, NOAA. Please note that this data series is not yet updated beyond 2018.

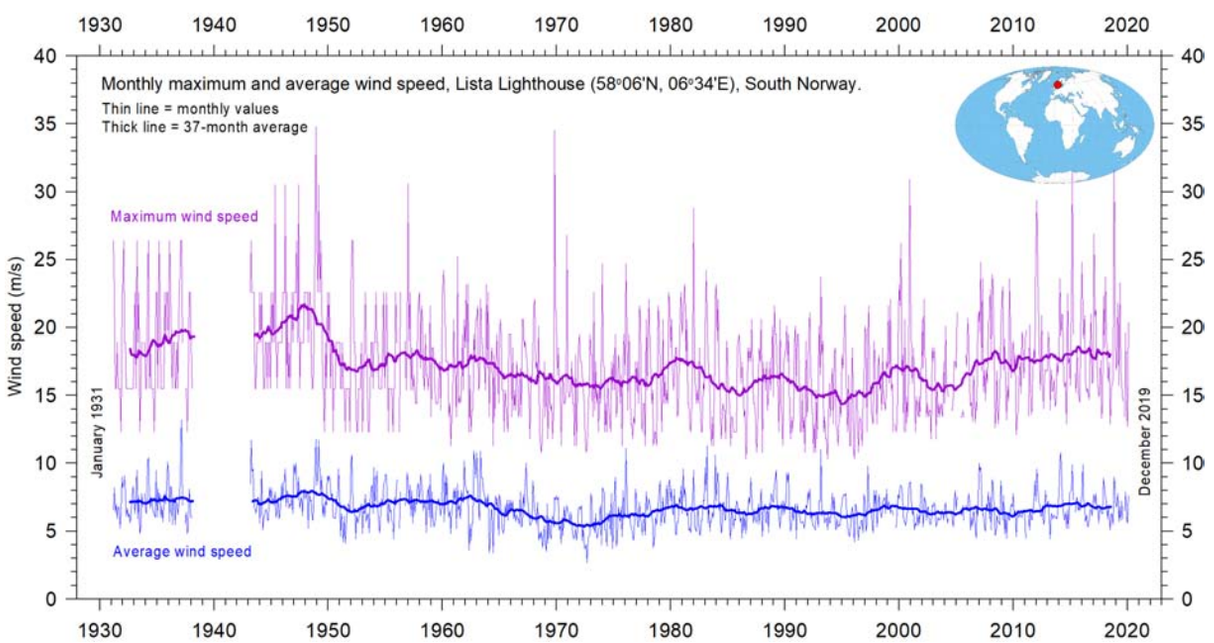

Figure 45: Wind speeds at Lista Lighthouse.

Source: eKlima.

Notes

1 See, for example Vignudelli et al., 2019.

2 Roemmich and Gilson 2009.

3 Carter et al. 2014.

4 Vignudelli et al., 2019 provide an updated overview of the current limitations of classical satellite altimetry in coastal regions.

5 See, for example, Turner et al., 2017 and Phys.org, 2019.

6 The ACE data and ongoing cyclone dynamics are detailed in Maue, 2011.

7 See Johnstone and Curry, 2017.

References

Papers cited

Carter R.M., de Lange W., Hansen J.M., Humlum O., Idso C., Kear, D., Legates D., Mörner N.A., Ollier C., Singer F. and Soon W. 2014. *Commentary and Analysis on the Whitehead & Associates 2014 NSW Sea-Level Report*. Policy Brief, NIPCC, 24. September 2014, 44 pp. http://climatechangereconsidered.org/wp-content/uploads/2014/09/NIPCC-Report-on-NSW-Coastal-SL-9z-corrected.pdf.

Chylek P., Folland C.K., Lesins G. and Dubey M.K. 2010. Twentieth century bipolar seesaw of the Arctic and Antarctic surface air temperatures. *Geophysical Research Letters*, 37, L08703.

Holgate S.J. 2007. On the decadal rates of sea level change during the twentieth century. *Geophysical Research Letters*, Vol. 34, L01602.

Johnstone J. and Curry J. 2017. *Causes and Predictability of the Exceptionally Active 2017 Atlantic Hurricane Season*. Climate Forecast Applications Network (CFAN). https://curryja.files.wordpress.com/2017/11/hurricane_review_2017-final.pdf.

Maue R.L. 2011. Recent historically low global tropical cyclone activity. *Geophysical Research Letters*, Vol. 38, L14803.

Roemmich D. and Gilson J. 2009. The 2004–2008 mean and annual cycle of temperature, salinity, and steric height in the global ocean from the Argo Program. *Progress in Oceanography*, 82, 81–100.

Turner et al. 2017. Unprecedented springtime retreat of Antarctic sea ice in 2016. *Geophysical Research Letters*, Vol. 44(13), p. 6868–6875.

Vignudelli et al. 2019. Satellite altimetry measurements of sea level in the coastal zone. *Surveys in Geophysics*, Vol. 40, p. 1319–1349. https://link.springer.com/article/10.1007/s10712-019-09569-1.

Data sources (accessed January–February 2020):

AMO, Earth System Research Laboratory, NOAA, USA: https://www.esrl.noaa.gov/psd/data/timeseries/AMO/.

Atlantic Oceanographic and Meteorological Laboratory, Hurricane Research Division: http://www.aoml.noaa.gov/hrd/tcfaq/E11.html.

Colorado Center for Astrodynamics Research: http://sealevel.colorado.edu/.

Danish Meteorological Institute (DMI): http://ocean.dmi.dk/arctic/icethickness/thk.uk.php.

Earth System Research Laboratory (ESRL): https://www.esrl.noaa.gov/psd/map/clim/olr.shtml.

eKlima: http://sharki.oslo.dnmi.no/portal/page?_pageid=73,39035,73_39049&_dad=portal&_schema=PORTAL.

GISS temperature data: https://data.giss.nasa.gov/gistemp/.

Global Marine Argo Atlas: http://www.argo.ucsd.edu/Marine_Atlas.html.

Goddard Institute for Space Studies (GISS): https://www.giss.nasa.gov/.

HadCRUT temperature data: http://hadobs.metoffice.com/.

Hurricane Research Division, NOAA: http://www.aoml.noaa.gov/hrd/tcfaq/E23.html.

National Ice Center (NIC). http://www.natice.noaa.gov/pub/ims/ims_gif/DATA/cursnow.gif.

National Snow and Ice Data Center (NSIDC): http://nsidc.org/data/seaice_index/index.html.

NCDC temperature data: https://www.ncdc.noaa.gov/monitoring-references/faq/.

Ocean temperatures from Argo floats: http://www.argo.ucsd.edu/.

Oceanic Niño Index (ONI): http://www.cpc.ncep.noaa.gov/products/analysis_monitoring/ensostuff/ensoyears.shtml.

Outgoing long wave radiation (OLR): https://www.esrl.noaa.gov/psd/map/clim/olr.shtml.

PDO, Joint Institute for the Study of the Atmosphere and Ocean (JISAO): http://research.jisao.washington.edu/pdo/PDO.latest.

Permanent Service for Mean Sea Level: http://www.psmsl.org/.

Phys.org 2019: https://phys.org/news/2019-01-antarctica-sea-ice-climate.html.

Plymouth State Weather Center: http://vortex.plymouth.edu/sfc/sst/.

PSMSL Data Explorer: http://www.psmsl.org/data/obtaining/map.html.

Rutgers University Global Snow Laboratory: http://climate.rutgers.edu/snowcover/index.php.

RSS temperature data: http://www.remss.com/measurements/upper-air-temperature.

Sea level from satellites: http://sealevel.colorado.edu/files/current/sl_global.txt.

Sea level from tide-gauges: http://www.psmsl.org/data/obtaining/map.html.

Sea ice extent Danish Meteorological Institute (DMI): http://ocean.dmi.dk/arctic/icethickness/thk.uk.php.

Southern Oscillation Index (SOI): http://crudata.uea.ac.uk/cru/data/soi/.

Tropical storm and hurricane accumulated cyclone energy (ACE): http://wx.graphics/tropical/global_ace.dat.

UAH temperature data: http://www.nsstc.uah.edu/data/msu/v6.0/tlt/uahncdc_lt_6.0.txt.

About the Global Warming Policy Foundation

The Global Warming Policy Foundation is an all-party and non-party think tank and a registered educational charity which, while openminded on the contested science of global warming, is deeply concerned about the costs and other implications of many of the policies currently being advocated.

Our main focus is to analyse global warming policies and their economic and other implications. Our aim is to provide the most robust and reliable economic analysis and advice. Above all we seek to inform the media, politicians and the public, in a newsworthy way, on the subject in general and on the misinformation to which they are all too frequently being subjected at the present time.

The key to the success of the GWPF is the trust and credibility that we have earned in the eyes of a growing number of policy makers, journalists and the interested public. The GWPF is funded overwhelmingly by voluntary donations from a number of private individuals and charitable trusts. In order to make clear its complete independence, it does not accept gifts from either energy companies or anyone with a significant interest in an energy company.

RECENT GWPF REPORTS

10	Whitehouse	The Global Warming Standstill
11	Khandekar	The Global Warming-Extreme Weather Link
12	Lewis and Crok	Oversensitive
13	Lewis and Crok	A Sensitive Matter
14	Montford, Shade	Climate Control: Brainwashing in Schools
15	De Lange, Carter	Sea-level Change: Living with Uncertainty
16	Montford	Unintended Consequences of Climate Change Policy
17	Lewin	Hubert Lamb and the Transformation of Climate Science
18	Goklany	Carbon Dioxide: The Good News
19	Adams	The Truth About China
20	Laframboise	Peer Review: Why Scepticism is Essential
21	Constable	Energy Intensive Users: Climate Policy Casualties
22	Lilley	£300 Billion: The Cost of the Climate Change Act
23	Humlum	The State of the Climate in 2016
24	Curry et al.	Assumptions, Policy Implications and the Scientific Method
25	Hughes	The Bottomless Pit: The Economics of CCS
26	Tsonis	The Little Boy: El Niño and Natural Climate Change
27	Darwall	The Anti-development Bank
28	Booker	Global Warming: A Case Study in Groupthink
29	Crockford	The State of the Polar Bear Report 2017
30	Humlum	State of the Climate 2017
31	Darwall	The Climate Change Act at Ten
32	Crockford	The State of the Polar Bear Report 2018
33	Svensmark	Force Majeure: The Sun's Role in Climate Change
34	Humlum	State of the Climate 2018
35	Peiser (ed)	The Impact of Wind Energy on Wildlife and the Environment
36	Montford	Green Killing Machines
37	Livermore	Burnt Offering: The Biomess of Biomass
38	Kelly	Decarbonising Housing: The Net Zero Fantasy
39	Crockford	The State of the Polar Bear Report 2019
40	Darwall	The Climate Noose: Business, Net Zero and the IPCC's Anticapitalism

For further information about the Global Warming Policy Foundation, please visit our website at www.thegwpf.org.

The GWPF is a registered charity, number 1131448.